2003

Solidification cracking susceptibility and microstructural development of Fe-Cu and Fe-Ni-Cu alloys

Fredrick F. Noecker II
Lehigh University

Noecker, Frederick F. II

Solidification Cracking Susceptibility and Microstructural Development of Fe-Cu...

January 2004

Solidification Cracking Susceptibility and Microstructural Development of Fe-Cu and Fe-Ni-Cu alloys

By

Fredrick F. Noecker II

A Thesis

Presented to the Graduate and Research Committee

Of Lehigh University

In Candidacy for the Degree of

Master of Science

in

Materials Science and Engineering

Lehigh University

5 December 2003

This thesis is accepted and approved in partial fulfillment of the requirements for the Master of Science

12 - 4 - 03

Date

Prof. John N. DuPont (Ph.D.)
(Thesis Advisor)

Prof. G. Slade Cargill III
(Chairman of Department)

ACKNOWLEDGEMENTS

The thanks due to the many that have made this thesis possible would be a thesis unto itself. Therefore, consider the following but an "abstract" for the thankfulness I have for so many that have given so much.

First, I would like to thank a man that was true to his word. About seven and a half years ago, as I was preparing to graduate from Lehigh and become a commissioned officer in the USAF, Prof. Marder gave me his word that if I ever wanted to attend graduate school, I would have a place working in his research group. If it were not for Prof. Marder's integrity, my family and I would not have been able to benefit from the tremendous opportunity the nearly past two and a half years have been for us. Additionally, Prof. Marder has provided words of wisdom during the inevitable irritants of graduate school that have made this experience more priceless than pearls.

So many thanks belong to Prof. DuPont, my mentor, teacher and guide. His profound patience for in helping me to relearn engineering after my five year active duty "hiatus" and reason enough for recognition! I have most appreciated learning from his profound engineering insight and keen eye for details that are too easily overlooked. The various projects we have worked on, including this thesis, have been invaluable to my gradual transformation into a researcher and engineer. However, he is more than an engineer or researcher. His love for family have been an example for me as I learn to balance the demands of research with the responsibility of husbandry of a home that will produce fruit long after my name is forgotten by the scientific community.

No acknowledgement would rightfully be complete without praising the excellent research engineers and staff in our department that make the pursuit of discovery

possible. Arlan Benscotter's ability to re-teach me metallography with patience, perseverance and an eye for excellence is commendable. What is just as commendable is his character and undying willingness to serve others. Arlan is a true leader in our department and a great man for he has always been willing to serve and help others.

On the first floor of Whitaker lab there resides three men whose literally provide a foundation of craftsmanship and technical expertise that enables the research in this department to be conducted. I would like to thank Mike Rex for his help in my experimental setup and his willingness to teach us how to weld through practical experience. The ability to quantitatively examine the microstructure and chemistry of materials would not be possible without the tireless efforts of Dave Ackland and Bill Mushok. Dave has more ears of experience with electron microscopes than I have years on this earth. His incredible memory bank of knowledge is invaluable in making sense out of the data collected from these very powerful machines. Bill's calm demeanor and ability to provide insight on the intricate workings of scanning electron microscopes has also been a tremendous help. These three men deserve thanks not only for their technical expertise, but also for their wit and humor, which never fails to brighten the day.

Next, thanks must be given to the Engineering Metallurgy Group (EMG), past and present. To Dr. Boris Levin, Dr. Don Susan, Dr. Steve Banovic, and Dr. Jesse Nawrocki. I want to thank you for your contributions to my undergraduate education and also to your continued input as research colleagues. You have left a heritage and tradition of engineering excellence, while remaining personable people, that we strive to uphold even to this day. I would like to thank my partner in LENS research, Dr. Weiping Liu for his profound technical insights into metal powder processing and for always taking the time

to provide a comment of encouragement when most needed. To Ryan "Pax-It Man" Deacon for putting up with the sulfidizing atmosphere I so readily produce in the office and invaluable metallographic technical resources. Your ability to listen, communicate and provide help whenever possible are hallmarks of the quality man that you are. To Matt Perricone, you are a profound young researcher with a passion for life and learning that reflect your physical size. Your willingness to lead, lend a helping hand and be completely honest with me is indicative of your moral fiber, which I am most thankful for. To John Regina who is most likely the wittiest, light hearted engineer I have ever met. John, your inborn, God given talent to teach is truly amazing. Thank you for taking the time to provide insightful feedback to the work I have shared with you. I would also like to thank past and present EMG members for their tremendous help, which I may never be able to repay. Dr. Chad Kusko, G. Phil Anderson, Heather Snow Moore, Ray Unocic, Shane Para, Susanna Kligensmith, Ken Adams, Tim Anderson and Mike Minicozzi, I want to thank you all.

My greatest thanks go to those who have sacrificed the most. Mom and Dad, your commitment to one another and to God has been a cornerstone in my life and person. Thank you for instilling in me a love for God, a passion for His creation and a deep seated desire to serve our country in whatever capacity I am lead into. In the years that lie ahead, I hope to be given opportunity to give back to you some of the love you have so freely given me. To my Grandma and PopPop Miller, thank your for your ceaseless prayers. May this and my future work bring honor to you.

To the flesh of my flesh and bone of my bones, Heather Renee, may have this opportunity to lift up your name in the "city gates". You are a Proverbs 31 woman, a

Sister in Jesus Christ, my 'ezer (Hebrew), the love of my life. Your loving respect and humble submission has enabled me to love and serve you in a Christ like way. Your companionship, prayers and love have filled me with such an incredible peace and joy that I can't even conceive how I lived life without you. You have sacrificed many nights and weekends so that this thesis could be written. It is to you that I dedicate it. I look forward to the future and eternity with you.

Most significantly, I would like to thank a very unordinary man for meeting me at my greatest point of need and rescuing me from the path of destruction my life had built. You are the Good Sheppard who has rescued this sheep by sacrificing your life so that I may not only have life, but have it more abundantly. I praise and thank you Jesus for giving me a second chance at life and love by granting me new birth. May your Name be praised!

Table of Contents

List of Tables

List of Figures

Abstract

The tool and die industry is interested in depositing Cu onto steel using direct metal deposition techniques in order to improve thermal management of mold dies manufactured from steel alloys. However, Cu is a known promoter of solidification cracking in steel. The goal of the first part of this work was to identify the range of Cu compositions in steel that cause cracking and understand the cracking susceptibility through analysis and modeling of microstructural development. A wide range of Steel - Cu deposits, from approximately 3 to 97 wt% Cu, were fabricated using the Gas Tungsten Arc Welding (GTAW) process with cold wire feed. The deposits were found to be crack free when the concentration of Cu was above approximately 52 wt% or below approximately 5 wt%. Cracking was observed in deposits with Cu concentration between approximately 5 and 43 wt%. Thus, one means to ensure crack free deposition of Cu onto Steel, the concentration of the first layer must be about 52 wt% Cu or greater. The corresponding volume fraction of terminal Cu in samples that cracked was between approximately 0.1 and 27%. The resultant microstructures were characterized by various microscopy techniques to understand the influence of Cu on solidification cracking. Additionally, solidification modeling was undertaken to determine the amount of terminal Cu rich liquid that would form under equilibrium and non-equilibrium solidification conditions. The second objective examined the range of Ni concentrations necessary to eliminate solidification cracking in Steel-Cu deposits and understand the cracking susceptibility through analysis and modeling of microstructural development. A wide range of Steel – Ni – Cu deposits, containing up to 75 wt% Ni, and Ni-Cu deposits were fabricated using the Gas Tungsten Arc Welding (GTAW) process with cold wire

feed. The Ni-Cu and Fe-Ni deposits were found to be crack free over the entire composition range. However, Ni concentrations of up to 75 wt% were insufficient to eliminate cracking when subsequent layers of Cu were deposited. Therefore, to ensure crack free deposition of Cu onto Steel, the concentration of the Ni interlayer must be greater than 75 wt% Cu. The resultant microstructures were characterized by various microscopy techniques to understand the influence of Ni and Cu on solidification cracking of Steel. Additionally, solidification modeling utilizing ThermoCalc was undertaken to determine the amount of terminal Cu rich liquid and solidification temperature range that would form under non-equilibrium solidification conditions.

Section I:

Microstructural Development and Solidification Cracking Susceptibility of Fe-Cu alloys

1-1. Introduction

Laser Engineered Net Shaping™ (LENS™) is a solid free form fabrication process capable of producing fully dense 3-D complex shapes directly from a Computer Aided Design (CAD) drawing via Direct Metal Deposition (DMD). LENS™ utilizes a Nd-YAG laser to produce a melt pool on a substrate attached to an X-Y table. Powder metal from coaxial powder feed nozzles is injected into the melt pool as the table is moved along a pre-designed two dimensional tool path that is "sliced" from a three dimensional CAD drawing. A fully dense part is produced by depositing line after line, which are built into sequential layers. LENS has already proven its ability to produce molds out of AISI H-13 Tool Steel[1] and has shown promise in producing conformal cooling channels in molds made out of the same material[2]. Additionally, several researchers have investigated the fabrication of functionally graded materials using DMD variant processes[3-5]. The tool and die industry would like to exploit the LENS process for producing Steel – Copper functionally graded conformable cooling channels to improve die thermal management and ultimately increase productivity.

AISI H-13 tool steel is a widely used mold material due to its favorable mechanical properties, but the thermal conductivity limits the melt cooling rate and increases mold cycle time. The thermal conductivity of copper[6] is approximately 13 times that of AISI H-13 tool steel[7] at operating temperatures between 220-600°C. It has been shown that mold cores fabricated from Cu based alloys used in steel molds significantly decrease the cooling times compared to monolithic H-13 tool steel[8].

Attempts to deposit copper onto H-13 tool steel using the LENS process have been limited in their success primarily due to solidification cracking[9]. Copper has been

shown by several researchers to promote solidification cracking/hot cracking in steel[10-13]. Solidification cracking is a function of the solidification temperature range and the amount of terminal liquid, both of which are controlled by the nominal composition and solidification conditions[14-17].

Figure 1 is an Fe-Cu equilibrium phase diagram[18], which displays a large solidification temperature range (ΔT) on the order of several hundred degrees C over a wide range of Cu concentrations along with limited solid solubility of Cu in Fe. The resultant effect on solidification cracking susceptibility is expected to be significant in both equilibrium and non-equilibrium solidification conditions. Under equilibrium solidification conditions (i.e. equilibrium at the solid/liquid interface, no undercooling and infinite diffusion in solid and liquid phases) Fe – Cu alloys with more than approximately 14 wt% Cu will produce terminal Cu rich liquid with a solidification temperature range of over approximately 300 °C. The unfavorably large solidification temperature range persists up to approximately 85 wt% Cu at which point the liquidus temperature decreases significantly and causes a considerable reduction in ΔT with increasing Cu. Solidification terminates when the liquid composition is enriched to pure Cu.

Non-equilibrium solidification conditions are similar to equilibrium conditions, except there is negligible diffusion of solute (Cu) in the solidifying solid (Fe) (otherwise known as the "Scheil" solidification condition[19]). For Scheil solidification conditions the large solidification temperature range is extended to even lower concentrations of Cu in Fe. If even trace amounts of Cu are added to Fe, solidification will terminate at pure Cu, with a solidification temperature range of over 400°C. Additionally, the limited solid

solubility of Cu in Fe will lead to significant amounts of terminal liquid over a similarly large range of nominal compositions. As such, the Fe-Cu system is expected to be inherently crack susceptible over a very large range of nominal compositions for both equilibrium and non-equilibrium solidification conditions. The objective of this work is to identify the concentrations of Cu in steel that result in crack free deposits as an important step towards successfully depositing Cu onto H-13 tool steel with the LENS™ process.

1-2. Experimental Procedure

A simplified, yet representative material system consisting of SAE 1013 steel and commercially pure deoxidized (DEOX) Cu were chosen to simplify the analysis while producing results representative of the solidification behavior of H-13 tool steel and copper. The compositions of the 1013 Steel and Cu wire are presented in Table I.

Single pass deposits provide the easiest means to analyze the effects of Cu concentration on solidification cracking. However, single pass deposits produced with the LENS™ process are on the order of only 1mm in width, making sample preparation and analysis difficult. The current work only considers compositional effects on solidification cracking Therefore, a wide range of Steel-Cu alloys were fabricated by depositing Cu onto 2.54 cm wide x 0.635 cm thick AISI 1013 rolled steel bar using a gas tungsten arc weld (GTAW) process with cold wire feed. The GTAW deposits are on the order of 1 cm in width or larger, permitting straight forward sample preparation and analysis, yet still representative of solidification under relatively high cooling rates.

The experimental setup is described in more detail by Banovic et.al.[20]. The GTAW processing parameters were as follows: 2.54 mm arc gap. 2 mm/s travel speed.

250 ampere arc current and 10 volt arc potential. The shielding gas was commercially pure Ar. The filler metal was 1.143 mm diameter (0.045 in.) deoxidized (DEOX) Cu. The deposit composition was varied by changing the wire feed speed, while all other processing parameters remained constant. Wire feed speed ranged from approximately 2 mm/s to 76 mm/s.

Transverse cross sections of samples from each processing condition were sectioned, mounted, ground and polished using standard metallographic techniques, then etched in 2% Nital. Both bulk and point compositions were determined with an electron-probe microanalyzer (EPMA). A JEOL 733 Super Probe, equipped with wavelength dispersive spectrometers, was operated at an accelerating voltage of 20 kV and a probe current of 25 nA for bulk analysis. To minimize the excitation volume yet maintain sufficient over-voltage to generate Cu K_α x-rays, the accelerating voltage was reduced to 15 kV for point analysis and line scans. To measure the nominal composition of the deposits three to six measurements were acquired per deposit from an area approximately 2000 μm^2 per measurement. This area was large enough to average out variations in composition due to microsegregation and provide good statistical measurement of the nominal deposit composition. A phi(ρZ) correction method was utilized to convert X-ray counts to weight percentages[21]. Compositional data was normalized for weight percent Fe and Cu, which is reasonable given the maximum amount of trace elements present is 1.36 wt%. For deposits with nominal Cu concentrations greater than 71 wt%, the geometric dilution method described by Banovic[20] was used to determine the nominal composition. Banovic[20] found that compositions of deposits measured by geometric dilution had good correlation (±2.4 wt%) to that measured by EPMA. Concentration

measurements were made with the EPMA when a higher degree of precision was required. Quantitative image analysis was used to perform geometric dilution and area fraction measurements. Area fraction was assumed equivalent to volume fraction. Twenty fields of view were measured for each deposit to provide good statistical confidence in the area fraction measurements.

1-3. Results

Steel – Cu deposits ranging in composition from 3.5 wt% to 97.0 wt% Cu were produced. The cracking susceptibility results for the Steel – Cu deposits are summarized in Figure 1 with solid and dashed lines corresponding to crack free and cracked deposits, respectively. Deposits with Cu concentrations up to 4.7 wt% Cu and greater than 51 wt% Cu were crack free. Solidification cracking was observed in deposits with Cu concentrations between 5.4 and 43.3 wt% Cu. The cracking susceptibility of deposits with Cu concentrations between 43.3 and 51 wt% Cu is unknown because there were no samples fabricated within this composition range.

Figure 2 is a micrograph of a 3.5 wt% Cu deposit. This deposit was crack free and remnants of the cellular solidification microstructure are apparent with bainite or martensite forming by solid state transformation due to the rapid cooling rate. The equilibrium solidification sequence for this Cu concentration would be liquid to delta ferrite. No Cu rich terminal phase was observed in this deposit.

A 6.1 wt% Cu deposit is shown in Figure 3. The deposit exhibited solidification cracking and a second phase with a spherical morphology was observed in the intercellular regions. Figure 4 displays EDS spectra obtained from the secondary phase and surrounding matrix, which confirms that the intercellular spheres observed in Figure

3 are indeed Cu rich. The x-ray excitation volume with a 20 kV accelerating voltage is approximately 1.5 microns in diameter, which is slightly larger than the spherical secondary phase and is most likely the reason why an Fe peak is observed in the EDS spectrum of the intercellular secondary phase. Sn is also observed in the Cu spheres due to the presence of Sn in the Cu wire (0.8 wt% Sn), which appears to partition to the Cu rich phase. The expected equilibrium solidification sequence is the same as the Steel – 3.5 wt% deposit, and the presence of Cu is not expected (under equilibrium solidification conditions). The intercellular Cu indicates that the solidification conditions deviate from equilibrium, which will be discussed in more detail in the subsequent section.

As the copper concentration in the deposit increases, the microstructure changes from cellular to columnar dendritic. Figure 5 is a micrograph of a 17.0 wt% Cu deposit. Cracking is observed along Cu rich regions of the deposit.

Another change in microstructure is observed as the Cu concentration is increased to 35 wt% Cu, as seen in Figure 6. The microstructure formed is the result of liquid phase separation that precedes solidification, resulting in a spinodal microstructure[22-24]. Like the 17 wt% Cu deposit (Figure 5), cracking is observed along the Cu rich regions of the deposit.

As the Cu concentration is increased, the spinodal microstructure becomes a fully interpenetrating network of Fe rich and Cu rich phases as seen in Figure 7 for 51.6 wt% Cu. This deposit and subsequent deposits with higher Cu concentrations were crack-free.

Figure 8 is a micrograph for 61.1 wt% Cu deposit that displays a combination of dendrites and liquid phase spinodal spheres in a Cu rich matrix. There is a change in the

spinodal microstructure from interpenetrating networks to spheres that exhibit a secondary phase separation similar to that reported by Elder[23].

1-4. Discussion

1-4-1. Solidification Behavior

Solidification conditions and the nominal composition control the solidification temperature range and amount of terminal liquid. Solidification cracking susceptibility is a function of the two latter quantities. Therefore, to understand cracking susceptibility it is necessary to determine the solidification behavior. Solidification behavior is bounded by equilibrium and non-equilibrium (Scheil) conditions. These two solidification conditions can be used to determine the upper and lower bounds for the amount of terminal liquid and the solidification temperature range.

To determine the solidification behavior of Fe – Cu alloys, and determine the amount of terminal Cu rich liquid that would form during solidification, the dimensionless back diffusion coefficient α must be calculated. Once the solidification behavior is known, the solidification temperature range and amount of terminal liquid can be determined.

It has been shown that microsegregation in welds is a function of the back diffusion potential of solute elements in the solidifying solid as the weld freezes[17,25-28]. Alloy systems with a small back diffusion potential will experience greater levels of microsegregation during solidification. The greater microsegregation will produce a larger amount of terminal solute rich liquid, which will impact the solidification cracking susceptibility of the alloy system.

In order to determine the solidification condition, the dimensionless back diffusion parameter (α) was calculated for the Fe-Cu system using the 6.1 wt% deposit. This sample will provide an upper bound estimate because the primary solidification phase is δ Fe, as it has a greater diffusivity of Cu than γ Fe[29]. Following the Brody-Fleming[28] solidification model, α is given by:

$$\alpha = \frac{D_s \, t_f}{L^2} \qquad [1]$$

where D_s is the diffusivity of the solute (Cu) in the solid (δ or γ Fe), t_f is the solidification time and L is the distance the solute must travel to eliminate any compositional gradient.

Because diffusivity is dependant on temperature and crystal structure of the solvent phase, the value of the back diffusion potential will change as the deposit cools. Therefore, an upper bound estimation is made for the back diffusion potential (α_{max}) of the 6.1 wt% Cu sample. If α_{max} is found to be << 1, then Fe – Cu alloys will solidify under non-equilibrium conditions regardless of temperature or crystal structure.

Diffusivity of Cu in δ Fe was found to be 7.9 X 10^{-12} (m^2/s) at 1500 °C[29]. This data provides an upper bound value for the diffusivity of Cu in δ Fe over the relatively narrow temperature range for δ Fe (1515 to 1485°C), assuming it solidifies under Scheil conditions, which will result in a larger solidification temperature range and upper bound estimation for α. As the 6.1 wt% alloy continues to cool, the γ Fe begins forming from the liquid at 1485°C. To provide the highest possible back diffusion potential in γ Fe, the diffusivity was calculated at the peritectic temperature, 1485°C, to be 7.6 X 10^{-14} (m^2/s) using the diffusion data provided by Arita[20].

L is equivalent to half the dendrite arm spacing since this represents the distance the solute atoms must travel to eliminate any concentration gradients in the forming solid. The average dendrite arm spacing was found to be 9.5 microns for the 6.1 wt% Cu sample.

Assuming a linear cooling rate during solidification, the solidification time, t_f, can be determined with the following equation:

$$t_f = \frac{\Delta T}{\varepsilon} \qquad [2]$$

where t_f is the solidification time, ΔT is the solidification temperature range and ε is the cooling rate.

To provide an upper bound estimate of the back diffusion potential in δ Fe, the temperature range (ΔT) between the liquidus and the Fe rich peritectic in the 6.1 wt% Cu alloy (1515 and 1485 °C) was used. Assuming the 6.1 wt% Cu alloy solidified under non-equilibrium conditions, back diffusion of Cu solute atoms would occur in γ Fe at temperatures below the Fe rich peritectic (1485 °C). The largest ΔT for γ Fe, which will result in the greatest amount of time for back diffusion, is the peritectic temperature (1485 °C) minus the Cu rich peritectic isotherm (1096 °C).

To estimate the cooling rate the Rosenthal equation for three dimensional heat flow from a point heat source was utilized[30]. Along the weld center line, the Rosenthal equation simplifies to:

$$\frac{\partial T}{\partial t} = \frac{2\pi\lambda S(T - T_o)^2}{\eta_a VI} \qquad [3]$$

where λ is the thermal conductivity, S is the travel speed, T is the temperature at which the cooling rate is estimated, T_o is the pre heat temperature, η_a is the arc transfer efficiency and VI is the arc power. The thermal conductivity for Fe at 727°C is 0.326 W/(cm °C). This was used as the effective thermal conductivity over the temperature ranges stated above. For the conditions used to make the deposits, VI = 2500 W, S = 0.2 cm/s, T_o = 25°C, T = 1515°C (the liquidus temperature for the 6.1 wt% Cu alloy) and η_a = .75 for the GTAW process[31]. Given the above conditions, the approximated cooling rate was found to be 485°C/s. For solidification as primary δ Fe, the solidification temperature range is 45°C, resulting in a solidification time of .09 seconds. Given the dendrite arm spacing of 9.5 microns, the resultant α = 0.0054, which is << 1, therefore back diffusion is negligible. If the primary solid was γ Fe, the maximum solidification temperature range would be 389°C, which is the Fe rich peritectic temperature (1485°C) minus the lower Cu rich peritectic temperature (1096°C). The estimated cooling rate would be 466°C/s, and the solidification time would be 0.83 seconds. Then α = 0.00070, which is also << 1 and even smaller than the back diffusion coefficient for solidification as primary δ Fe. Even though the solidification time is greater for γ Fe, the diffusivity is nearly two orders of magnitude less than that for δ Fe. Therefore, negligible back diffusion will occur during solidification, indicating that the solidification conditions are expected to be close to non-equilibrium "Scheil" conditions.

It should be noted that the cooling rate is an estimate for two reasons. First, the Rosenthal solution is based on the assumption of a point heat source. In practice, the GTAW heat source is not a point heat source but rather, more diffuse, which will result in

lower cooling rates. Secondly, cooling rate is a function of temperature. The cooling rate decreases with decreasing temperature. Assuming the actual cooling rate is only half that predicted by the Rosenthal equation, α_{max} for δ and γ Fe are 0.011 and 0.0014 respectively. Non-equilibrium conditions persist even if cooling rate is decreased by half.

As such, it can be concluded that the presence of the copper spheres in the 6.1 wt% sample (Figure 3) is a result of non-equilibrium solidification conditions. However, the absence of terminal Cu in the Steel – 3.4 wt% Cu sample (Figure 2) is evidence that some back diffusion of Cu did occur to prevent the formation of terminal Cu at this nominal composition. Based on these two microstructures, and the back diffusion calculations, the solidification conditions are close to non-equilibrium, but some limited diffusion does exist.

The solidification behavior of the 6.1 wt% Cu alloy is representative of the solidification behavior for the entire Fe – Cu system. This can be seen by considering how the parameters that effect α change with Cu concentration. If Cu concentration is increased slightly beyond 6.1 wt%, the solidification temperature range in δFe decreases. This will decrease α for concentrations up to 8.1 wt% Cu, which is the maximum concentration at which the primary solid phase is δFe. For Cu concentrations greater than 8.1 wt%, the primary solidification phase changes from δ to γ Fe and resultant diffusivity decreases by nearly two orders of magnitude, thereby significantly reducing α. This is true even though the solidification temperature range, which effects solidification time, is greater in γ Fe than it is in δ Fe. As Cu concentration is increased beyond 8.1 wt%, the solidification temperature range decreases, further reducing the back diffusion

potential of Cu in Fe. Given the effects of increasing Cu concentration on t_f, and D_s, the entire Fe – Cu system is expected to exhibit near Scheil solidification conditions.

Assuming the solidification conditions are non-equilibrium for all Steel – Cu alloys, there will be an even greater range of nominal compositions with large solidification temperature ranges. The influence of solidification conditions on solidification temperature range is given in Figure 9. Under equilibrium conditions the solidification temperature range is quite small up to the Fe rich peritectic (8.1 wt% Cu). As the nominal composition of Cu increases beyond 8.1 wt% the equilibrium solidification temperature range is less straightforward due to the shape of the γ solidus. Because the austenite solidus extends out to approximately 13 wt% Cu before bending back to 8.2 wt% Cu, the equilibrium solidification sequence will occur by initial solidification, followed by remelting, then resolidification at the Cu rich peritectic isotherm. This is the case for equilibrium solidification of alloys with nominal Cu concentrations ranging from approximately 8 to 13 wt%. In Figure 9, the line representing the equilibrium solidification temperature range ignores the initial solidification and remelting phenomenon, thereby displaying an upper bound range of compositions with a solidification temperature range on the order of hundreds of degrees C. The solidification temperature range for equilibrium and non-equilibrium solidification conditions will be the same (liquidus – melting point of pure Cu) when the nominal composition of the deposit is greater than approximately 13 wt% Cu. With Scheil solidification conditions, the range of nominal compositions with solidification temperature range on the order of several hundred degrees C is increased to even trace amounts of Cu. This is because the terminal reaction during non-equilibrium

solidification is pure Cu over the entire range of nominal compositions in the binary phase diagram.

Figure 9 also displays the range of nominal compositions that experienced solidification cracking, which correlates reasonably well with the range of compositions where the solidification temperature range is very large. At approximately 43 wt% Cu another factor comes into play, the amount of terminal liquid available for backfilling of cracks.

The amount of terminal liquid is the other key variable in solidification cracking susceptibility. The terminal liquid is defined as the volume of liquid present at the end of solidification. This terminal liquid transforms to the Cu rich phase at the end of solidification. The amount of terminal liquid can be determined by measuring the amount of Cu in the deposits. The volume fraction measurements for the deposits are presented in Figure 10. The 95% confidence interval was used to calculate error bars for each point. Cracking was observed in deposits that contained between 0.1 and 27 vol. % terminal Cu.

Given that the deposits solidify under non-equilibrium Scheil conditions, the measured amount of terminal Cu can be compared to the predicted amount as calculated by the Scheil equation. To predict the amount of terminal Cu the differential form of the Scheil equation must be used because the equilibrium partitioning coefficient, k, is not constant in the Fe-Cu system. The differential Scheil equation is given by:

$$df_S = \left(\frac{1 - f_S}{C_L - C_S^*} \right) dC_L \qquad [4]$$

where df_S and dC_L are the infinitesinamal change in fraction solid and liquid composition respectively. C_L and C_S^* are the composition of the liquid and the solid, respectively, at the solid liquid interface at any temperature given by the equilibrium liquidus and solidus lines from the Fe-Cu phase diagram. Equation 4 enables the fraction solid (and corresponding fraction liquid) to be calculated by use of a finite difference method for any given nominal composition.

When using the finite difference method, the starting conditions are: $f_S = 0$, $C_L = C_O$ at the liquidus temperature, and C_S^* is given by the solidus composition at the liquidus temperature. The value of dC_L was set to 1 wt% Cu. The values for C_L and C_S^* are read directly from the equilibrium phase diagram. The fraction solid formed at any temperature below the liquidus is found by repeatedly solving Equation 4 for each dC_L and summing the resultant values of df_S to provide fraction solid at any temperature. The finite difference technique provides the mass fraction of solid (f_S). The mass fraction liquid, f_L, is then given by $f_L = 1 - f_S$. For the case of the Fe – Cu system, the differential Scheil calculation was carried out until the Cu rich peritectic isotherm was reached since all liquid that reaches the Cu rich peritectic (96.7 wt% Cu) will be transformed to the Cu rich phase (95.9 wt% Cu and greater). This can be seen in the Fe-Cu phase diagram in Figure 1.

To determine the volume percent terminal Cu for Scheil solidification conditions, the f_L, which is in weight fraction, must be converted to volume percent by a modification of the lever rule:

$$V_{Cu} = \frac{\frac{f_{L,Cu}}{\rho_{Cu}}}{\frac{f_{L,Cu}}{\rho_{Cu}} + \frac{f_{S,Fe}}{\rho_{Fe}}} X\ 100 \qquad [5]$$

where $f_{L,Cu}$, $f_{S,Fe}$, ρ_{Cu} and ρ_{Fe} are the weight fraction and room temperature density of Cu and Fe respectively. Using Equation 5, the resultant values for volume percent terminal Cu as predicted by the differential form of the Scheil equation are presented in Figure 11 as the "Scheil Solidification Model" line. The volume fraction terminal liquid can be determined using the finite difference Scheil technique given the assumption that the equilibrium phase boundary lines are known and that the solidifying liquid follows these boundaries as it is cooled. This is expected to provide a good approximation for Cu concentration between 3.5 and 22.5 wt%. The presence of a liquid phase spinodal decomposition in deposits with Cu concentration 35 wt% and greater results in a change of phase boundary lines that does not allow the iterative Scheil technique to be used. The liquid phase spinodal decomposition will be discussed more in the next section. Also in Figure 11 are the measured values of Cu rich phase from deposits with Cu concentration up to 22.5%, with error bars that represent the 95% confidence interval for both composition measurements with the EPMA and volume fraction measurements with QIA.

Additionally, the expected amount of terminal Cu under equilibrium solidification conditions, assuming all subsequent diffusion ceased at the end of solidification, is presented as the "Equilibrium Solidification" line. These results are determined by the lever rule at the Cu rich peritectic isotherm temperature (1096°C) to determine the fraction terminal Cu rich phase. In this calculation, the Fe rich solid phase was taken

from the equilibrium phase diagram to be 8.2 wt% Cu and the Cu rich liquid phase was given by 96.7 wt% Cu. The liquidus composition at the Cu rich peritectic (96.7 wt%) was used to represent the amount of terminal Cu because all liquid that reaches the Cu rich peritectic isotherm will transform to the Cu rich solid phase. The weight fraction terminal rich Cu was then converted to volume percent using Equation 5.

The second equilibrium line, "Room Temp Equilibrium", displays the room temperature volume percent of Cu as determined by the equilibrium binary Fe-Cu phase diagram at room temperature. These values were calculated with data from the Fe-Cu phase diagram at 600°C, which shows negligible solid solubility of Fe and Cu in each other.

The unique shape of the Fe – Cu phase diagram produces an unexpected result in the solidification modeling as seen in Figure 11. For any nominal composition greater than the Fe rich peritectic (8.1 wt% Cu), non-equilibrium solidification results in less terminal Cu rich liquid than for equilibrium solidification conditions. This is due to the shape of the γ solidus line. As an alloy cools below the Fe rich peritectic temperature, the solid solubility of Cu in austenite increases to approximately 14% at 1400°C. However, below this temperature, during equilibrium solidification, the entire solid begins rejecting Cu solute into the liquid. In the Scheil condition, Cu solute is "locked" into the pre-existing solid due to the negligible diffusivity of Cu in austenite. The result is less Cu solute present to form terminal liquid in the Scheil condition.

In eutectic systems, the opposite occurs, with Scheil conditions acting as an upper bound for the amount of terminal liquid[17]. In a eutectic system, the solidus and liquidus slopes are of the same sign over the entire solidification temperature range and the

composition of the solid continues to increase until the maximum solid solubility is reached at the eutectic isotherm. This results in the largest amount of solute being rejected into the liquid when solidification occurs under Scheil conditions. In the Fe – Cu system the solidus and liquidus slopes are no longer of the same sign over the entire solidification temperature range. The solidus slope starts negative, then becomes positive as temperature decreases while the liquidus slope remains negative. The result is a decreased amount of terminal Cu rich phase when solidifying with Scheil conditions.

The significance is that both the equilibrium and Scheil solidification calculations predict less solid Cu rich phase at room temperature than the equilibrium room temperature results. This is due to the assumption that there is no diffusion of Cu in Fe at the end of solidification, which was made in both the Scheil and Equilibrium solidification models.

Because the Fe – Cu system has a low back diffusion potential, it is expected that both the equilibrium room temperature and equilibrium solidification calculations would not accurately predict the amount of terminal second phase. There is reasonably good agreement between the Scheil prediction and the experimental data. Yet there is a slight over prediction of the amount of terminal Cu using the Scheil calculation compared to the measured volume percent for any given nominal composition. There are two possible reasons for this. Firstly, the deposits fabricated in this work contains elements other than Fe and Cu, therefore, the phase boundary lines for the Steel – Cu deposits may be shifted as compared to the binary Fe – Cu system. Secondly, dendrite tip undercooling can enrich the composition of the first solid to form, resulting in less terminal solute rich liquid than predicted by the Scheil results[32]. To investigate this possibility, an EPMA

line scan across the cellular structure in the Steel – 6.1 wt% alloy was acquired (Figure 12). The line scan spans the cellular structure and intersects with a terminal Cu rich sphere. Because the size of the sphere is approximately the same size as the X-Ray emission volume, it is not possible to quantitatively determine the composition of the interdentric Cu rich phase with the EPMA technique, however, the composition profile across the cell can provide information on how the composition of the solid changed during solidification. The portion of the EPMA line scan in Figure 12 representing the cell core to the intercellular region is shown in Figure 13 and compared to the Scheil results where the cell core is taken as $f_S=0$ and the interdendritic region, where the Cu concentration peaks, is taken as $f_S=1$. Note that the experimental data has a higher composition Cu than that predicted by the Scheil model for any amount of fraction solid. This is most likely a result of dendrite tip undercooling or a shift in phase boundary lines.

1-4-2. Liquid Phase Separation

Another potential indicator of undercooling is the presence of liquid phase spinodal. According to the Fe – Cu binary phase diagram with metastable miscibility lines[33] (Figure 14), a certain amount of undercooling is required for the liquid phase separation to occur. The amount of undercooling is dependent upon nominal composition. Liquid phase spinodal structures were seen for alloys ranging from 35 to 71 wt% Cu, which corresponds to a minimum undercooling ranging from 54 to 32°C respectively. The amount of undercooling not only effects the composition of the first solid to form and whether the liquid phase separation occurs, it also decreases the solidification temperature range and solidification cracking susceptibility concomitantly.

As discussed in the Results section, there is a significant change in microstructure between the 17 and 35 wt% Cu deposits (Figure 5 and Figure 6 respectively). This provides one indicator of a liquid phase separation and subsequent spinodal decomposition in the Fe-Cu system, which has been reported by several researchers[22]. Another evidence is the composition of the Fe rich and Cu rich phases of the spinodal. EPMA measurements were made of the Fe and Cu rich phases of the spinodal microstructure and are given in Table II. These results are in good agreement with the experimental results of Nakagawa[34] and Elder[23] as compiled by Chen[35].

There are two distinct types of liquid phase spinodal structures observed. The first type consists of an interpenetrating Fe rich and Cu rich networks that are continuous throughout the fusion zone. Figure 7 is an example of this morphology, which is very similar to that observed by Zeng[22], but with a larger wavelength due to the lower cooling rates in GTAW deposition as compared to laser surface alloying used by Zeng. This first structure was observed in deposits with nominal compositions ranging from 35.0 – 55.3 wt% Cu.

A second type of spinodal structure is seen as the nominal composition of Cu increases (Figure 8), which correspond to spinodal structures observed by Elder[23]. Figure 15 is an SEM micrograph of a liquid phase spinodal sphere observed in the 61.1 wt% Cu deposit. EDS was used to determine that the matrix is Cu rich and the spheroid with perturbations is Fe rich with Cu rich spheres within the Fe rich outer ring (Figure 16). All three EDS spectra were taken under the same conditions for the same count time and are plotted on the same scale, allowing for qualitative comparisons to be made. The EDS spectra of the secondary sphere is nearly identical to that of the matrix, with only

slightly more Fe and Mn, most likely due to the excitation of the surrounding Fe rich sphere. The morphology of this second type of spinodal structure providence some evidence on how the Fe – Cu liquid phase spinodal solidifies.

It has been suggested[23] that the solidification sequence would begin with the Fe rich liquid phase due to the greater undercooling this phase would experience at any given undercooling at the nominal composition. The solidification of the Cu rich phase would then follow. This hypothesis is supported by the spherical spinodal microstructures seen in Figure 8 and Figure 15. Fe rich perturbations are seen extending from the spheroid that has undergone secondary phase separation[23], where Cu rich spheres are seen within an Fe rich sphere surrounded by a Cu rich matrix. The presence of the Fe rich perturbations suggests that the Fe rich phase does indeed solidify first, with post liquid phase separation growth of the Fe rich phase into the Cu rich liquid phase.

1-4-3. Cracking Susceptibility

The solidification cracking susceptibility of Steel – Cu deposits can be understood by combining the solidification temperature range estimates (Figure 9) and the volume percent terminal Cu data (Figure 10). At Cu concentrations below approximately 5 wt% the estimated Scheil solidification temperature range is greater than 400°C but no terminal Cu is observed. The absence of terminal Cu indicates that the deposit did not solidify completely under Scheil conditions and that there was some finite amount of back diffusion. The absence of terminal Cu also indicates that the solidification temperature range for deposits with less than 5 wt% Cu is less than that predicted using the Scheil solidification conditions. The deposit is crack free due to the lack of terminal Cu and most likely a reduced solidification temperature range.

The estimated solidification temperature range, under Scheil solidification conditions, for deposits with nominal Cu concentrations between approximately 5 and 43 wt% remains greater than 350°C, and terminal Cu is present. The large solidification temperature range and intermediate amounts of terminal Cu produces solidification cracking. As the Cu concentration continues to increase beyond 43 wt%, the solidification temperature range continues to decrease and the amount of terminal Cu continues to increase. The increased terminal Cu is sufficient to backfill any cracks that may form during solidification.

GTAW deposits may present a worst case cracking susceptibility scenario when compared to laser deposition. In work performed by Zeng, Cu was laser surface alloyed onto SAE 1045 steel producing a melt zone with nominal composition of 33 wt% Cu[22], in which no cracking was observed[36]. The same composition deposit fabricated using GTAW resulted in cracking, with the nominal composition lying well within the high crack susceptibility region. The microstructures observed in the current work are analogous to Zeng's but of a much coarser scale as would be expected due to slower relative cooling rate in GTAW processes as compared to laser surface alloyed composites.

In general, if Cu is to be deposited onto steel using arc welding processes, the first layer must contain at least 50 wt% Cu to avoid solidification cracking. A second potential solution is to use an interlayer material that exhibits good solid solubility and a small solidification temperature range when alloyed with Cu or Fe. The potential of using Ni as such an interlayer is explored in a future publication.

1-5. Conclusion

To determine the compositional cracking range of Cu in Steel, a wide range of Steel – Cu deposits were fabricated by GTAW with a cold wire feed. EPMA measurements were carried out to determine the composition of the Steel – Cu deposits. Deposits with compositions ranging from 5.4 to 43.3 wt% Cu were found to be crack susceptible, while compositions above 51.5 and below 4.7 wt% Cu were found to be crack free.

Solidification cracking was found to be a function of both the solidification temperature range and the amount of terminal Cu rich liquid. Cracking occurred when the solidification temperature range was between 349 to 436°C and when the amount of terminal Cu was between 0.1 and 26.9 volume percent. Solidification calculations utilizing a finite difference Scheil technique and the binary equilibrium Fe – Cu phase diagram provided reasonable estimates of the amount of terminal Cu during solidification. The current work may provide a more conservative estimate of solidification cracking susceptibility as compared to laser deposition.

1-6. Individual tables

Table I: Compositions of AISI 1013 bar and DEOX Cu wire

	C	Mn	Si	S	P	Cr	Ni	Mo	Cu	Fe	Al	Sn
Cu wire	-	0.18	0.23	-	0.01	-	-	-	98.78	-	-	0.8
SAE 1013 Bar	0.13	0.82	0.173	0.02	0.007	0.026	0.066	0.015	0.08	98.643	0.009	0.011

Table II: Phase Compositions of Spinodal Structures

Nominal Composition	Phase	
	Fe rich	Cu rich
	wt% Cu	*wt% Cu*
Steel - 16.7 wt% Cu	11.28	92.455
Steel - 35.0 wt% Cu	13.563	93.231
Steel - 37.9 wt% Cu	12.716	90.779
Steel - 50.5 wt% Cu	16.598	88.428
Steel - 55.3 wt% Cu	15.474	94.777
Steel - 69.5 wt% Cu	17.743	92.096

1-8. Figures

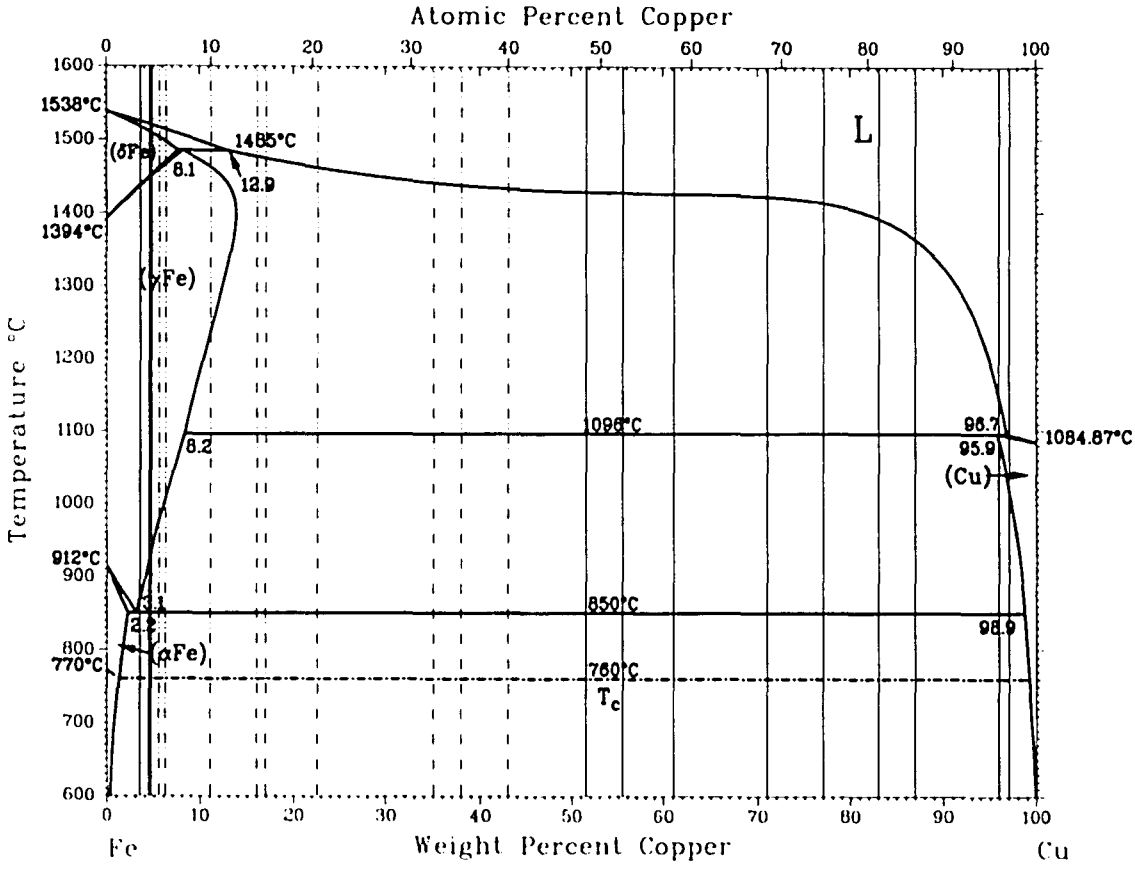

Figure 1: Fe-Cu equilibrium phase diagram[18] with solidification cracking results. Solid and dashed lines represent crack free and cracked deposits respectively

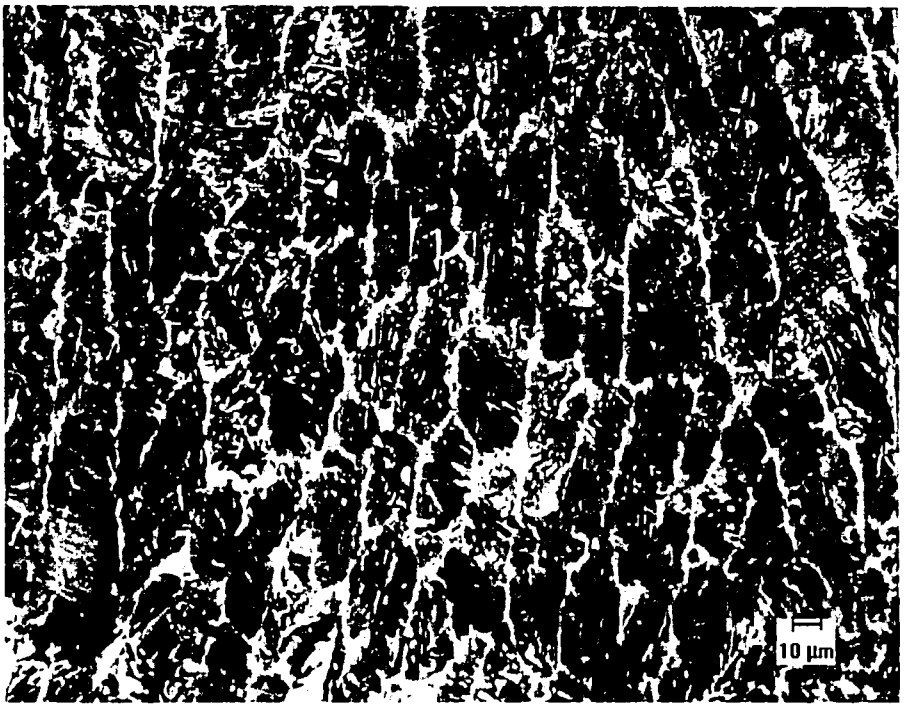

Figure 2a and b: Steel - 3.5 wt % Cu

Figure 3a and b: Steel - 6.1 wt% Cu. Terminal Cu in intercellular regions

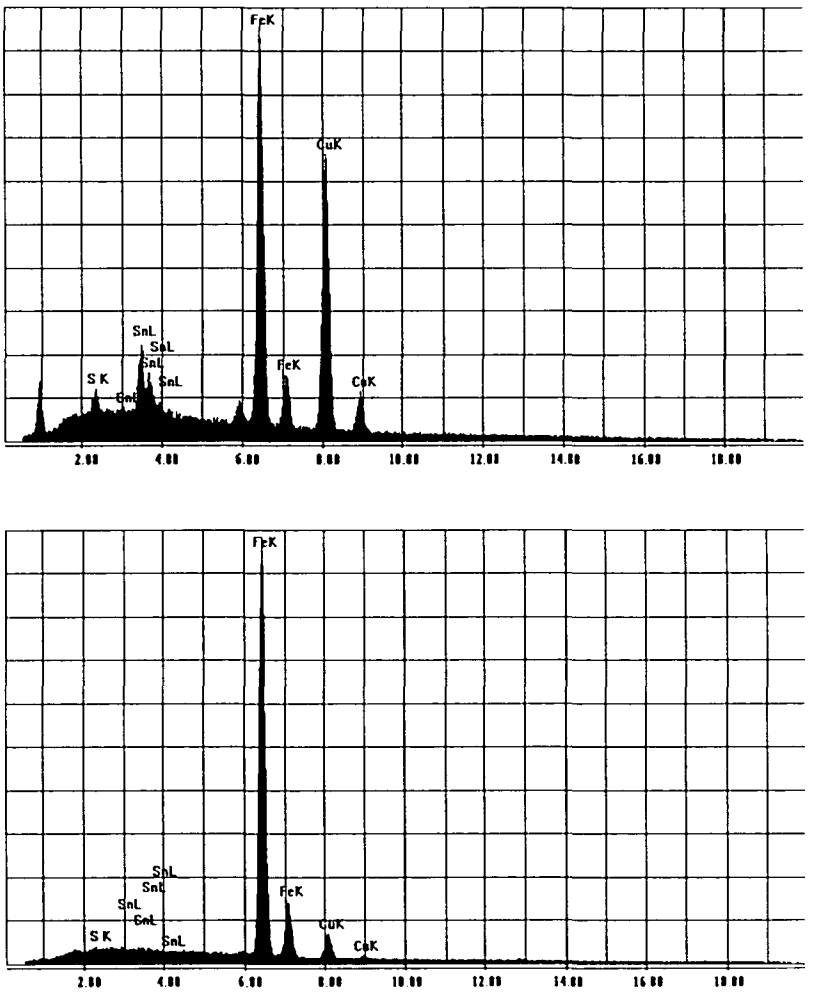

Figure 4: EDS spectra of a) intercellular sphere, b) surrounding matrix, in Steel - 6. 1 wt% Cu

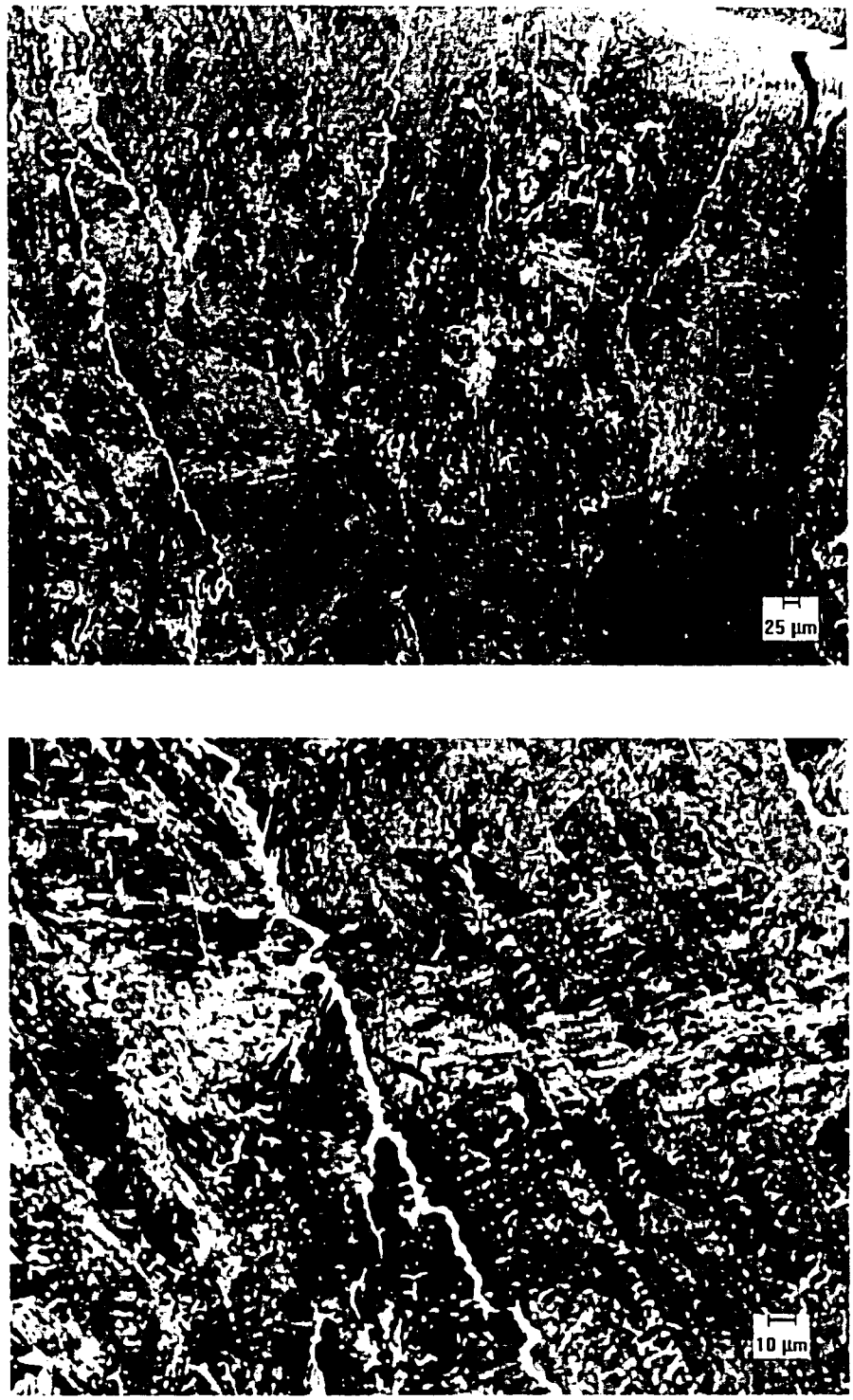

Figure 5a and b: Steel - 17.0 wt% Cu. Columnar dendritic substructure with cracking occurring along Cu rich interdendritic regions

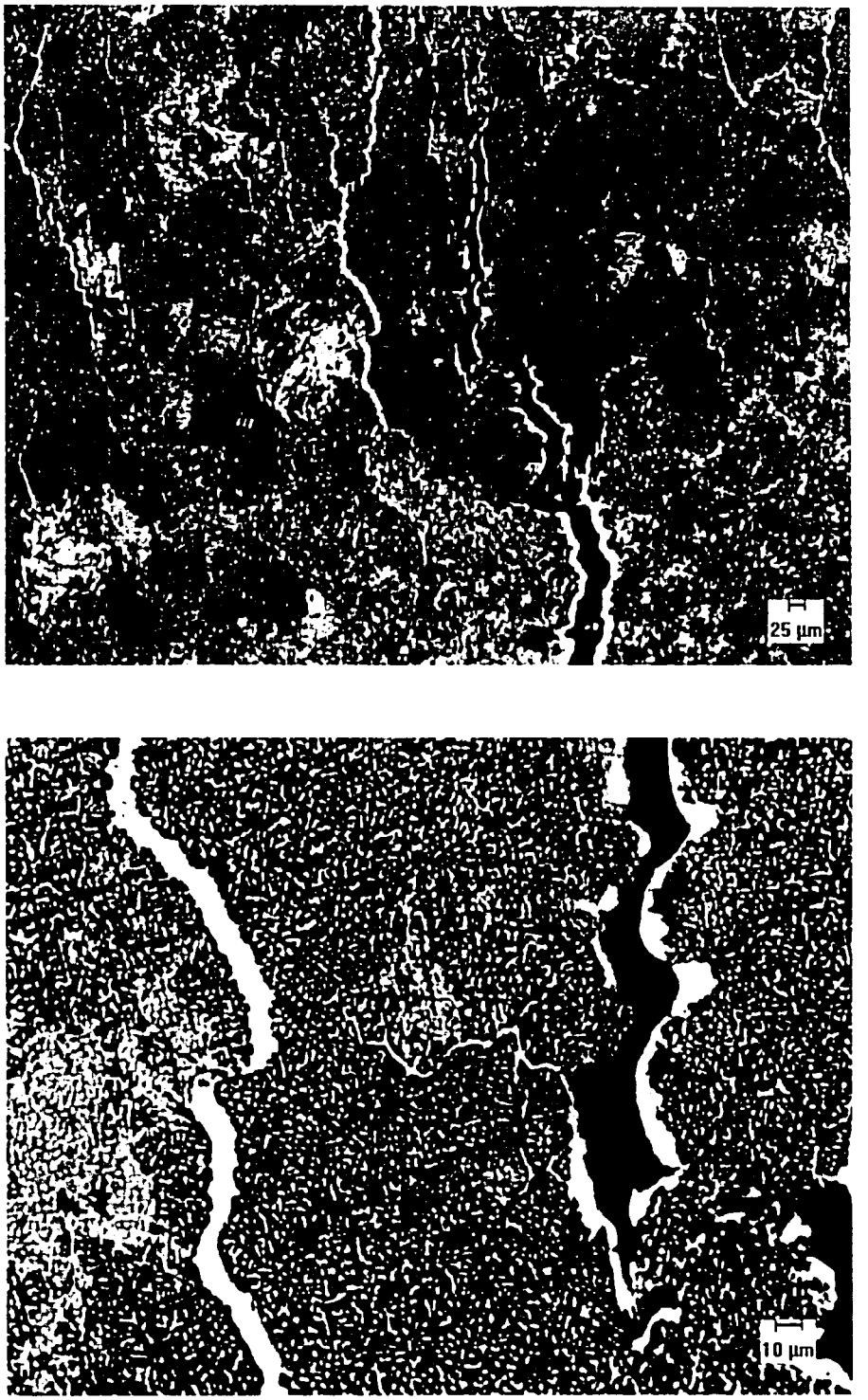

Figure 6 a and b: Steel - 35.0 wt% Cu. Liquad phase spinodal structure with cracking along Cu rich regions

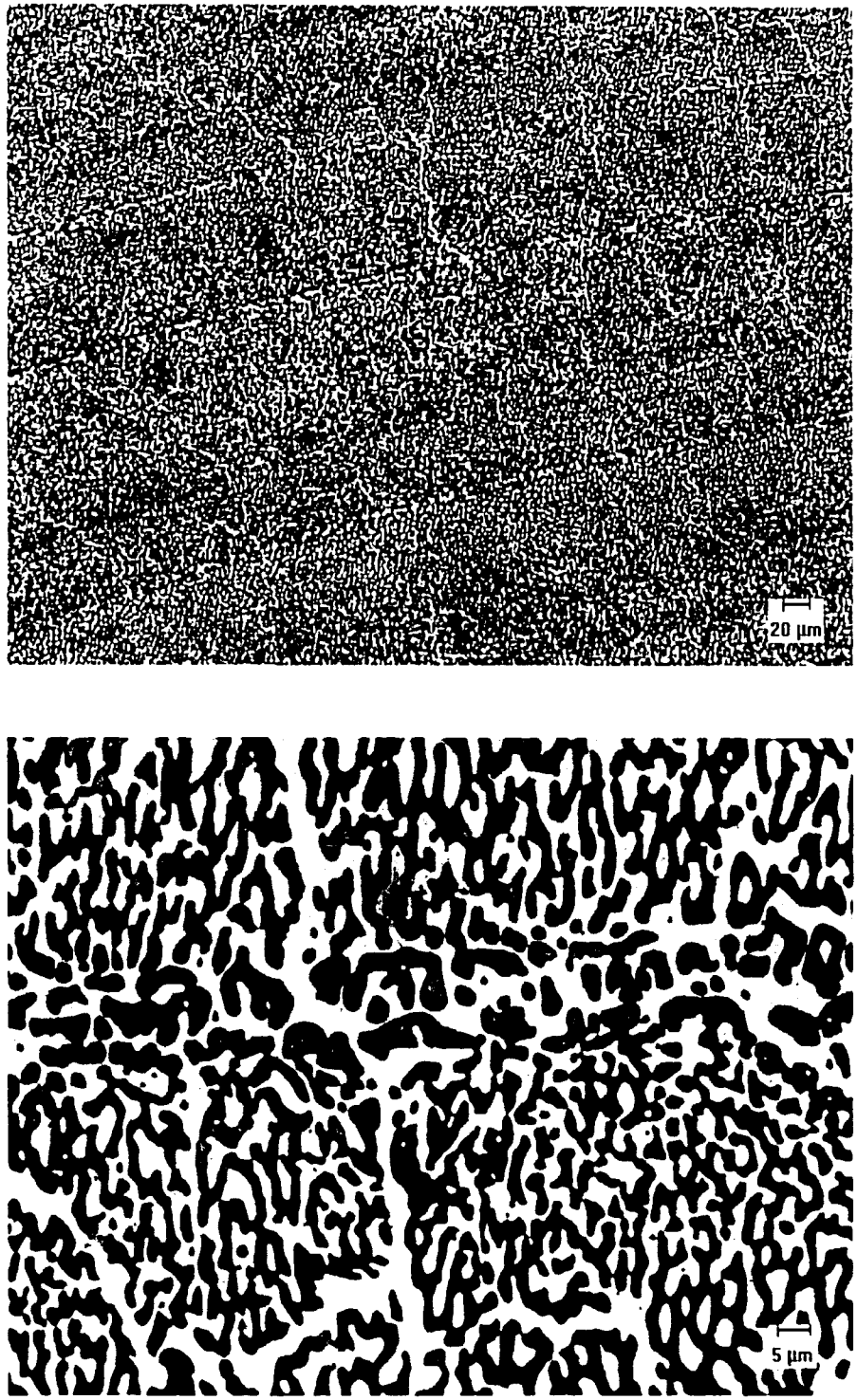

Figure 7 a and b: Steel - 51.6 wt% Cu. Fully interpenetrating Fe rich (dark) and Cu rich (light) networks in liquid phase spinodal structure that is crack free

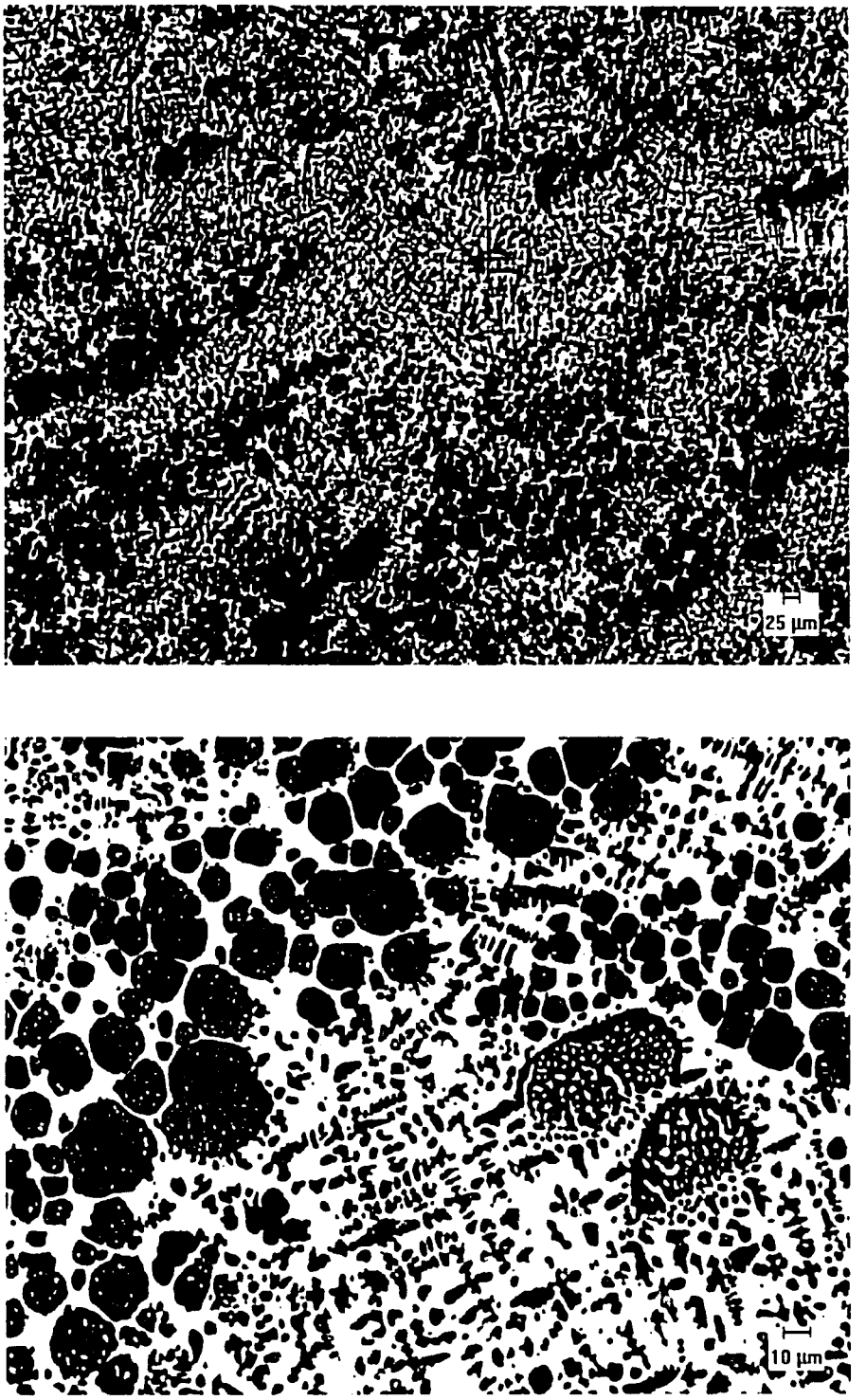

Figure 8 a and b: Steel - 61.1 wt% Cu. Spheroid liquid phase spinodal structures amongst equiaxed dendritic structures that are crack free

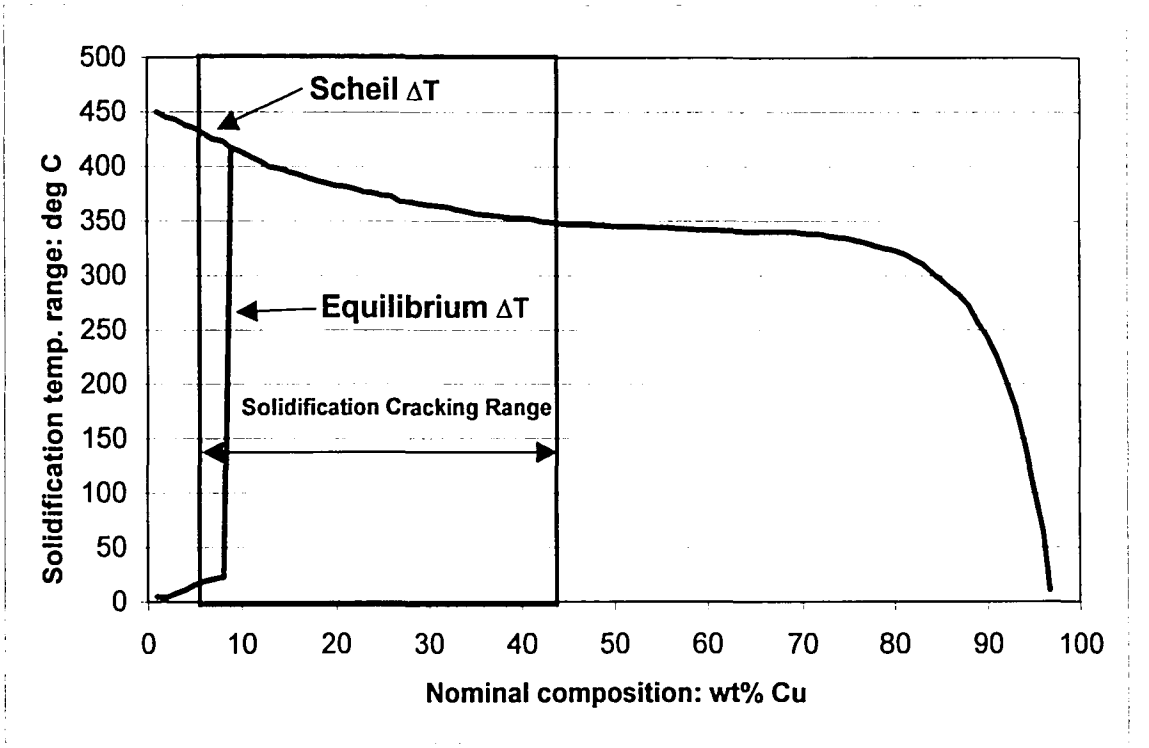

Figure 9: Solidification temperature range for equilibrium and Scheil solidification conditions. At Cu concentrations greater than 8 wt% the solidification temperature range is for Equilibrium and Scheil solidification conditions are the same and the two lines overlap. Crack susceptible range of compositions indicated by arrow

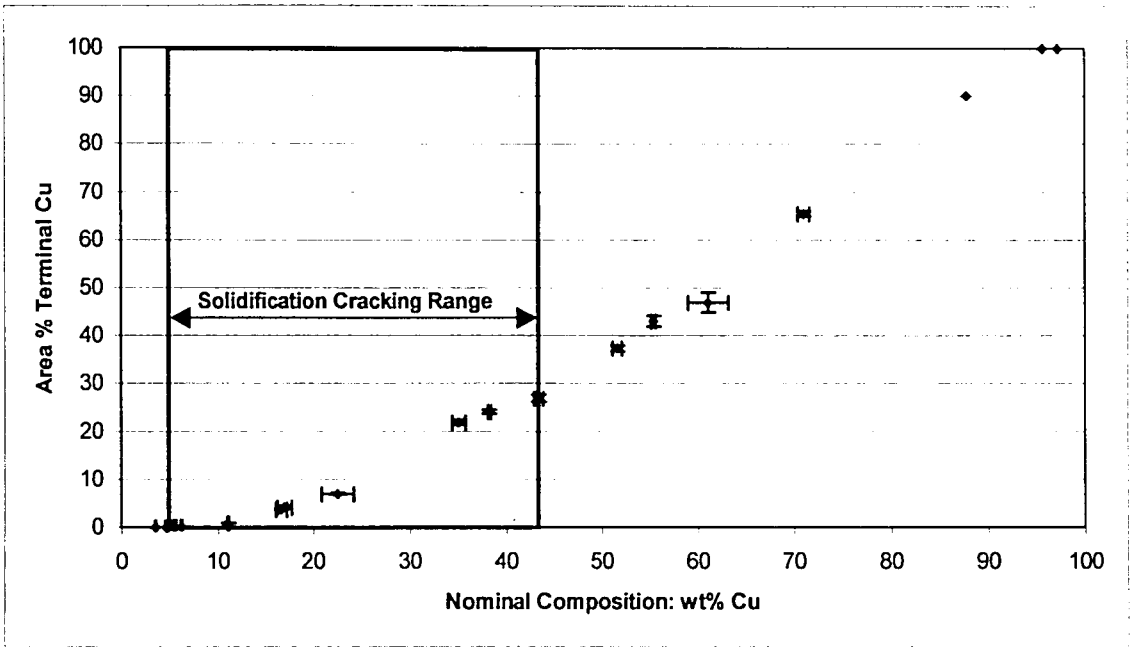

Figure 10: QIA measured amounts of terminal Cu. Crack susceptible range of compositions indicated by arrow

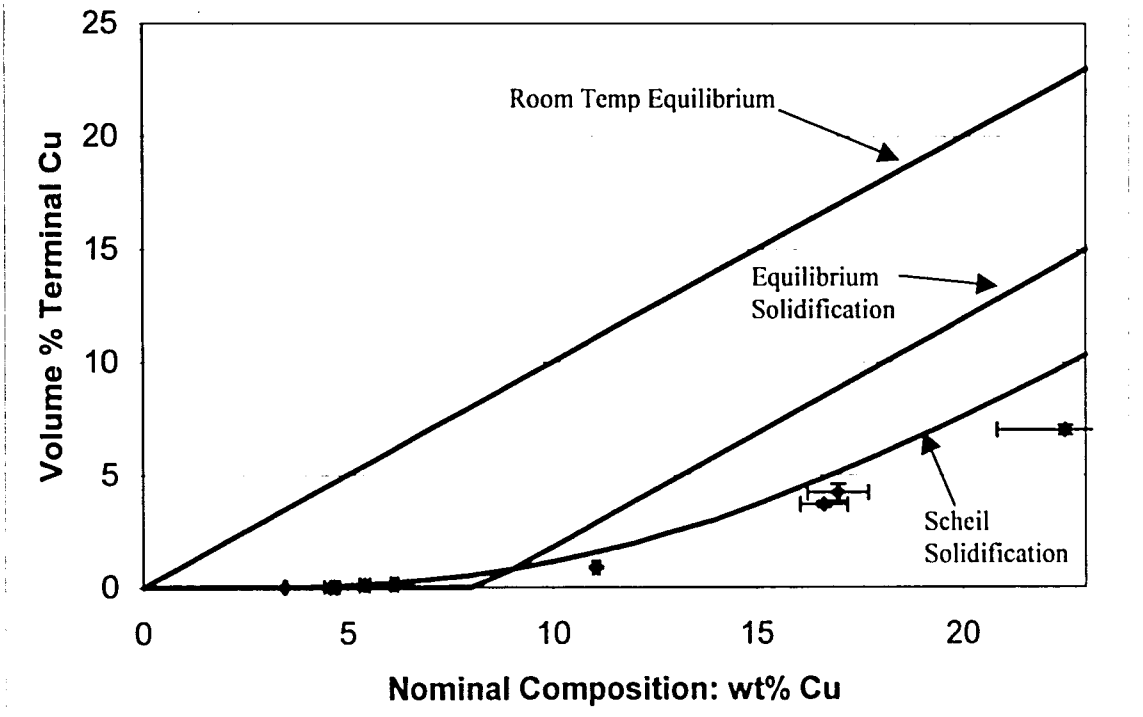

Figure 11: Volume percent terminal Cu calculated under several different conditions compared to QIA measured amounts of terminal Cu

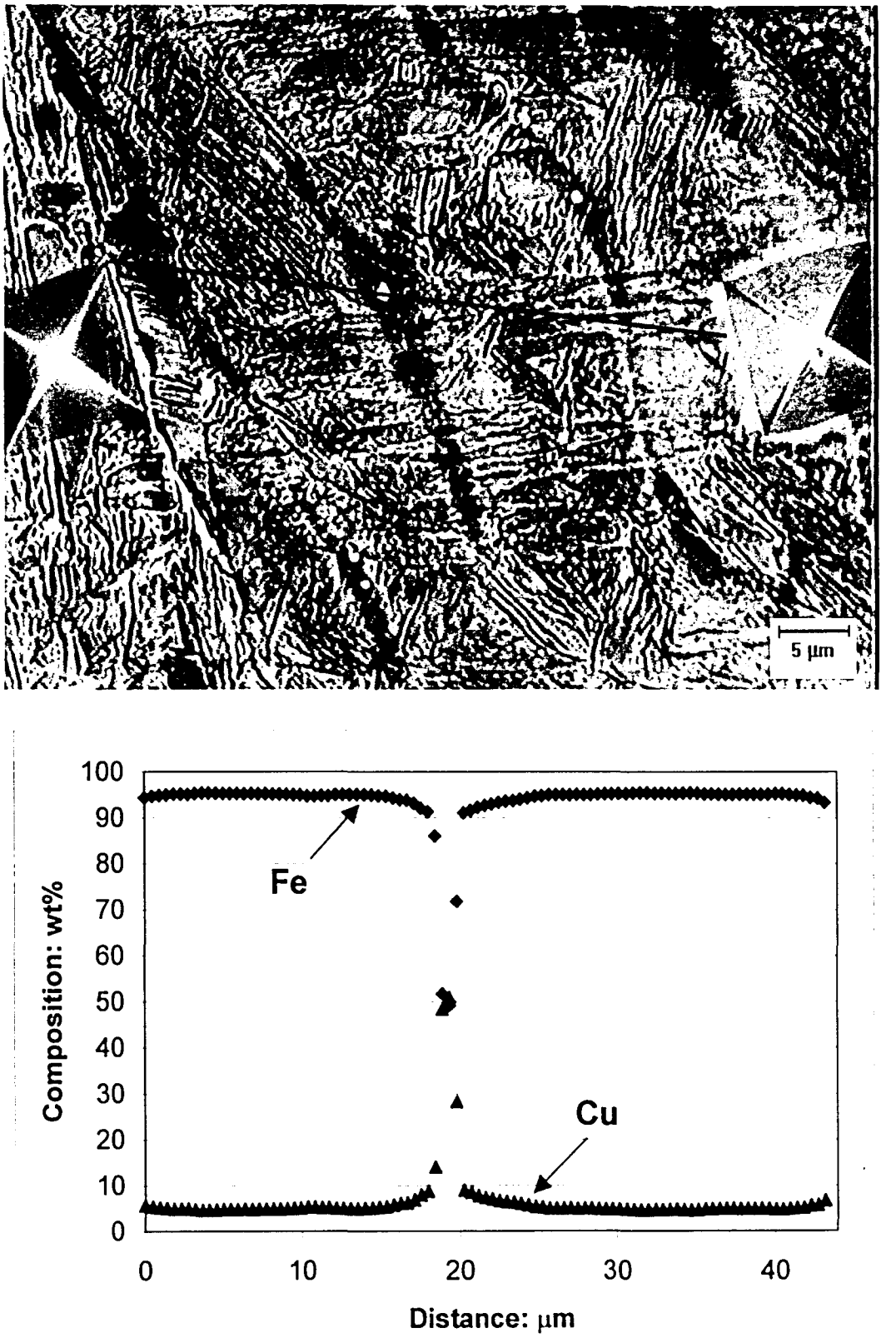

Figure 12: a) Steel - 6.1 wt% sample with b) EPMA line scan

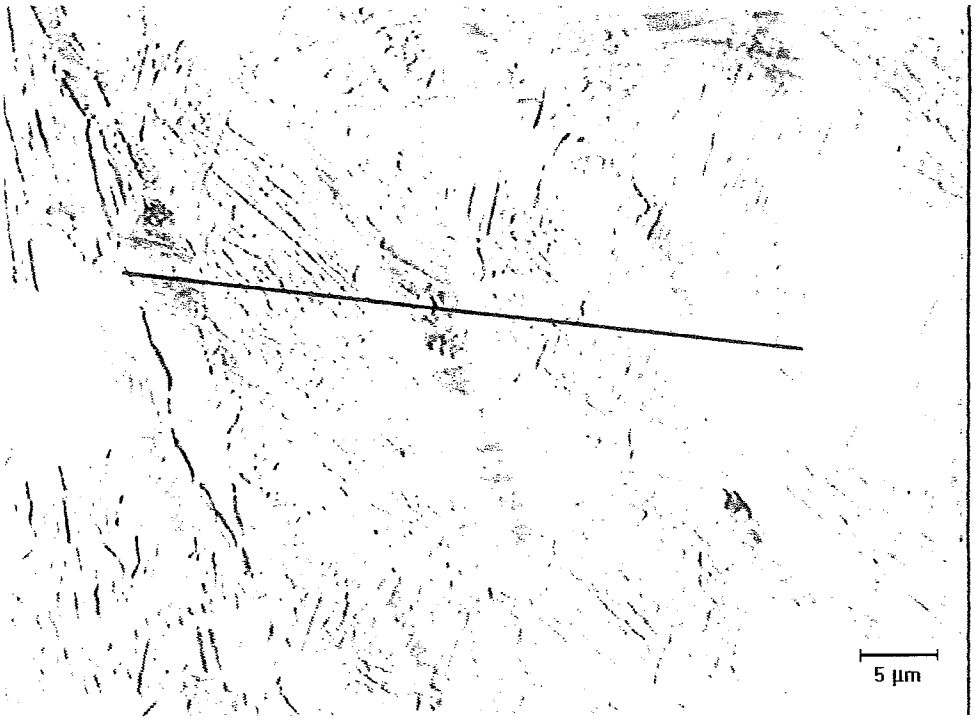

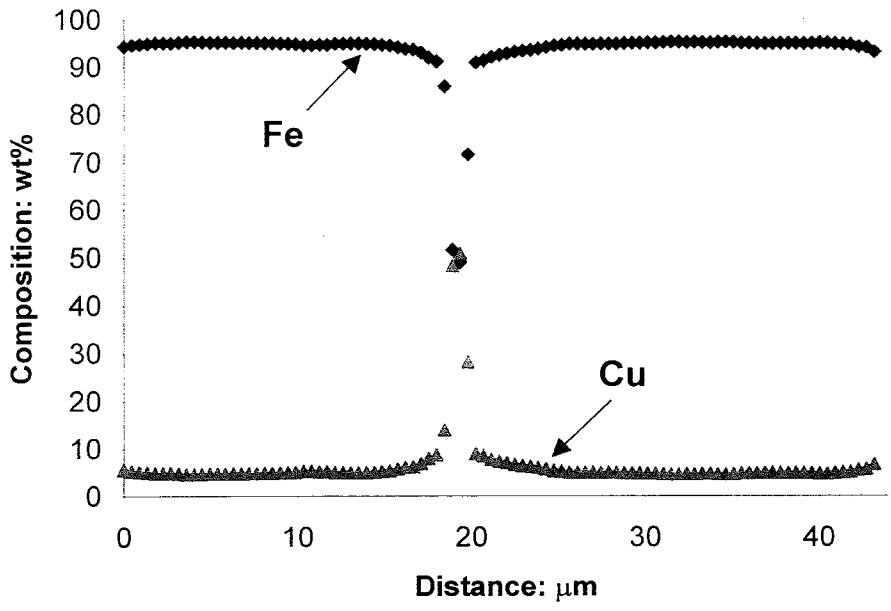

Figure 12: a) Steel - 6.1 wt% sample with b) EPMA line scan

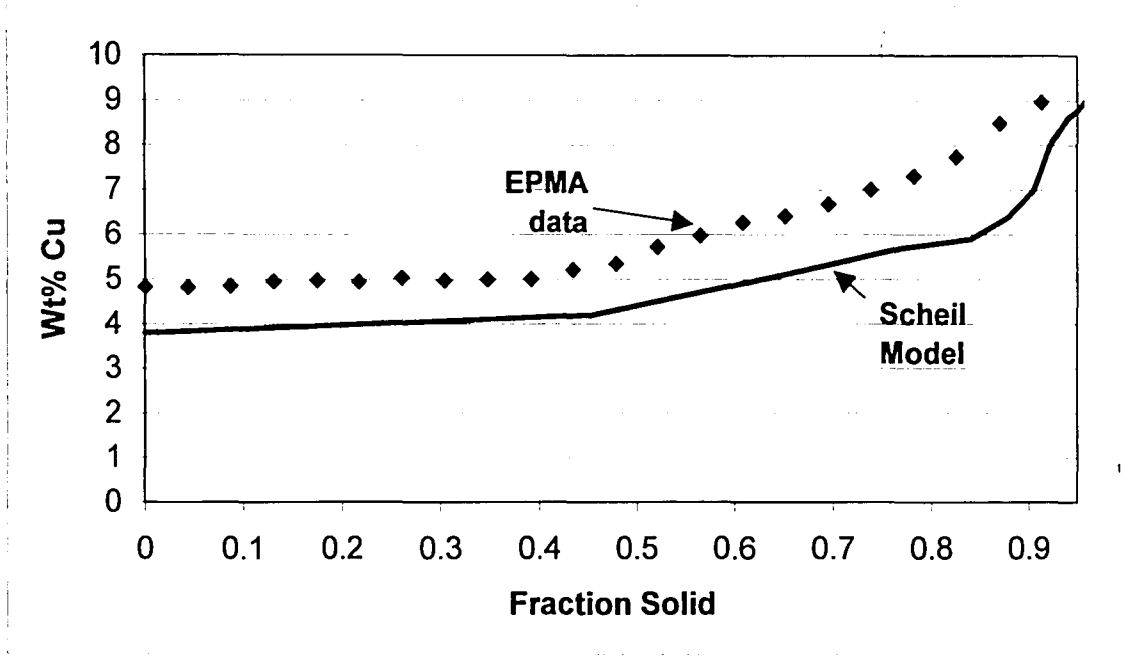

Figure 13: Composition of Cu from the cell core to intercellular region in 6.1 wt% Cu sample compared to Scheil predicted composition

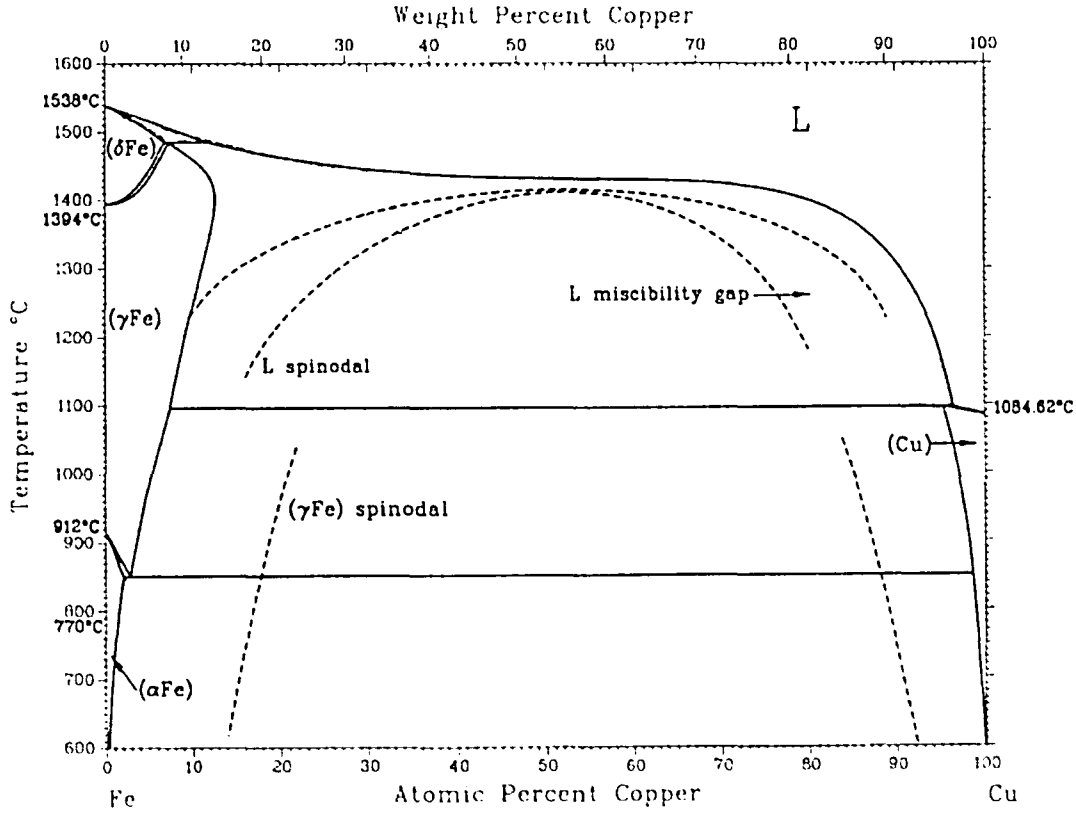

Figure 14: Fe-Cu phase diagram with metastable miscibility lines[33]

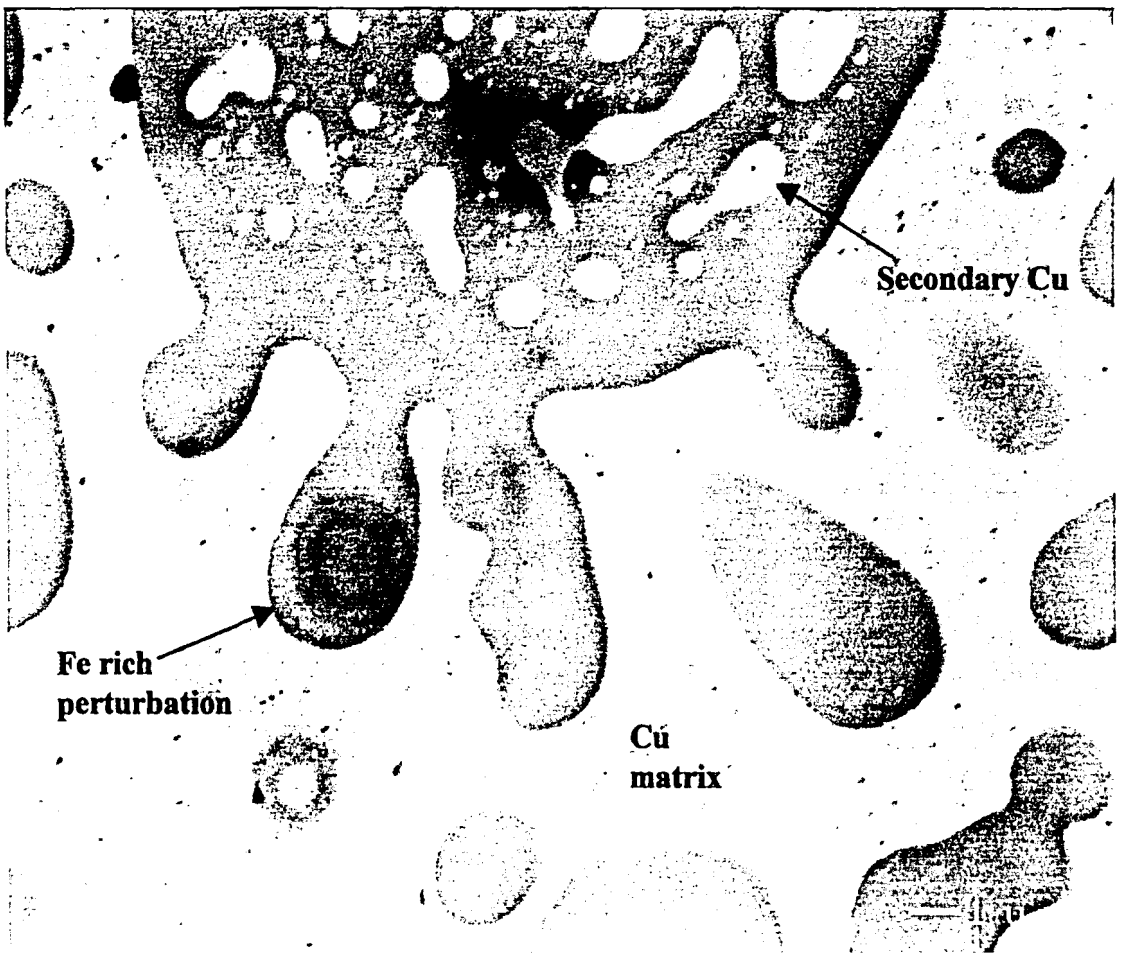

Figure 15: SEM image of a spinodal sphere in 61.1 wt% Cu that displays secondary phase separation and dendritic growth of Fe rich sphere into Cu rich liquid upon solidification

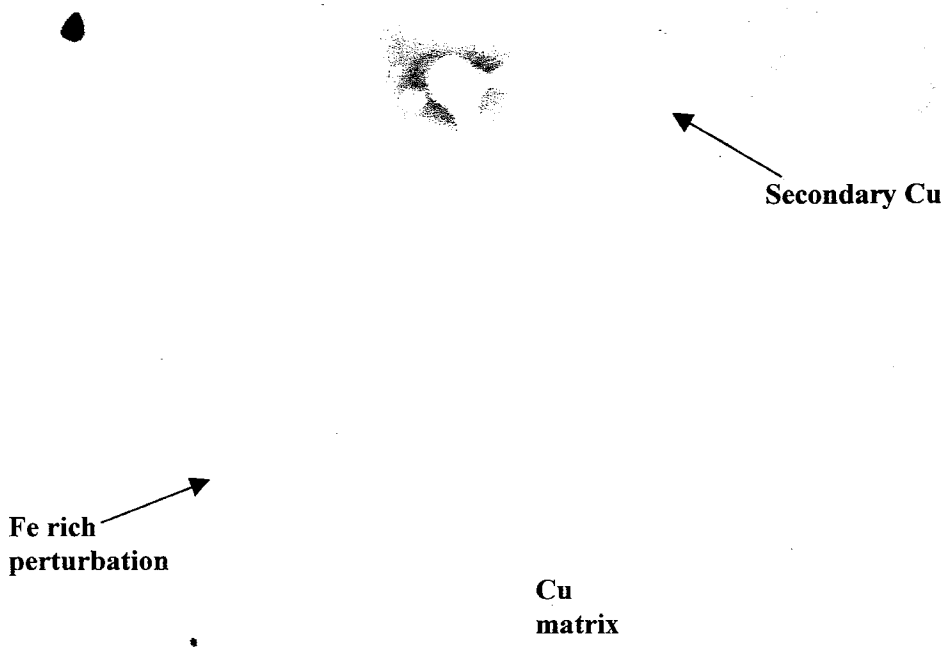

Figure 15: SEM image of a spinodal sphere in 61.1 wt% Cu that displays secondary phase separation and dendritic growth of Fe rich sphere into Cu rich liquid upon solidification

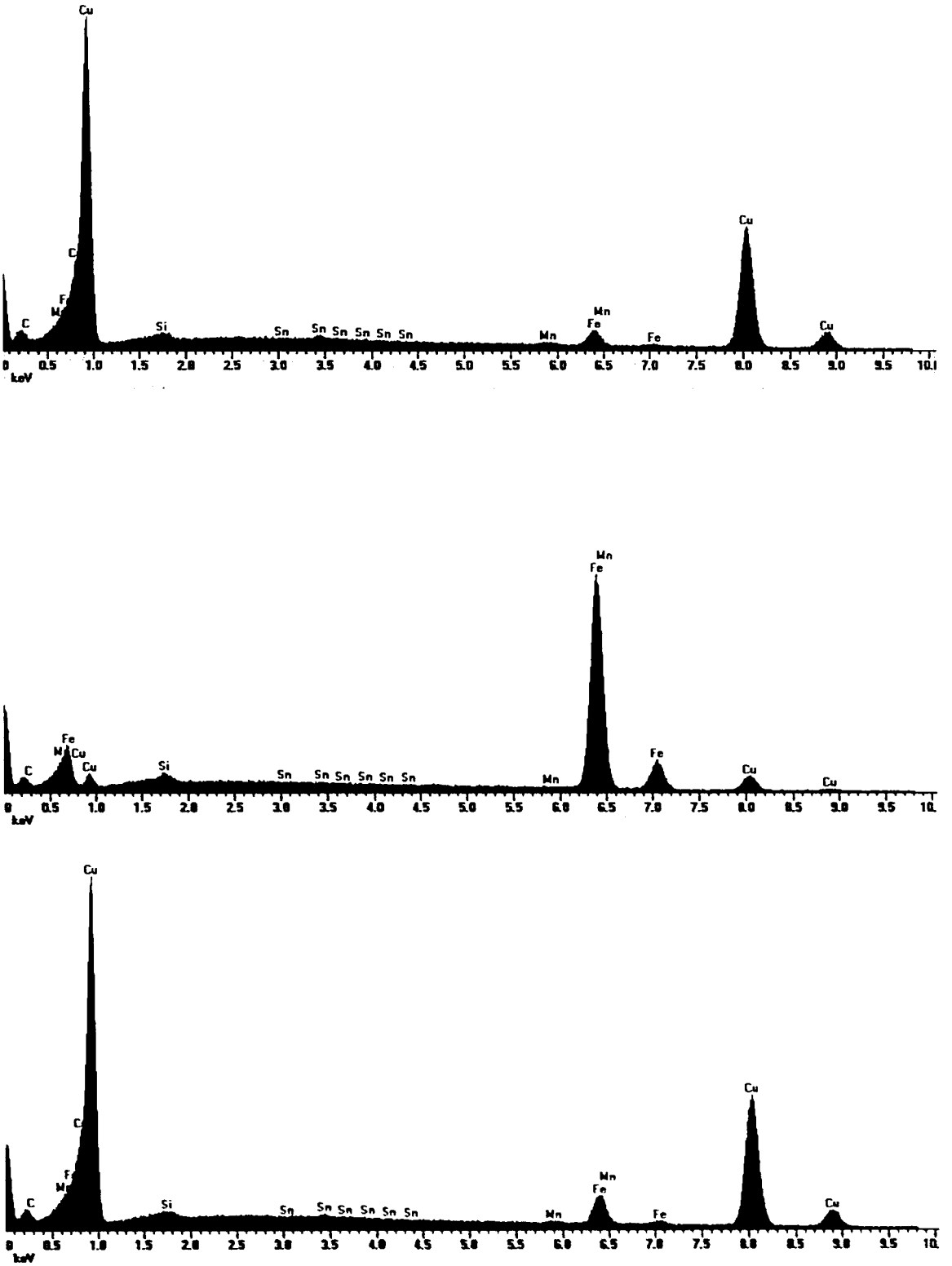

Figure 16: EDS spectra of spherical spinodal structure: a) matrix surrqunding structure b) Fe rich portion and c) Cu rich portion of structure

Section II:

Microstructural Development and Solidification Cracking Susceptibility of Fe-Ni-Cu alloys

2-1. Introduction

Direct metal deposition processes offer the unique advantages of producing fully dense three dimensional metallic parts directly from a computer aided design drawing. As such, the tool and die industry would like to harness the advantages of direct metal deposition processes to fabricate molds with functionally graded compositions in order to improve mold performance. One possible means to improve the thermal conductivity of H-13 Tool Steel molds is to selectively deposit Cu using a compositional gradient. The thermal conductivity of Cu is nearly 13 times greater than H-13 tool steel[6,7], and its use in this application would translate into shorter mold cycle times and increased mold productivity.

However, copper has been shown by several researchers to promote solidification cracking/hot cracking in steel[10-13]. Attempts to deposit Cu onto H-13 tool steel using a direct metal depositions process have also been hampered by solidification cracking[9]. Additional work that used AISI 1013 Steel and Cu as a model system examined the effects of Cu concentration on solidification cracking. Solidification cracks were found to form in deposits with Cu concentration between 5 and 43 wt% (Section I).

Two primary metallurgical controlling factors in solidification cracking are the solidification temperature range and the amount of terminal liquid at the end of solidification. Nickel has been shown to increase the solubility of Cu in austenite[37], which should result in a concomitant reduction of the amount of terminal Cu rich liquid and solidification cracking susceptibility. Several researchers have found that the addition of Ni, either as an interlayer or as an alloying element with Cu, decreases the cracking susceptibility when Cu is deposited on Steel[38-40]. The addition of Ni is also

expected to improve the thermal conductivity of the molds, due to its thermal conductivity being more than twice that of H-13 [6].

The equilibrium phase diagrams for Fe-Ni and Cu-Ni are given in **Figure 17**[41]. The Fe-Ni phase diagram exhibits a very small solidification temperature range. Additionally, it is nearly isomorphous, with almost complete solid solubility at elevated temperatures, and would therefore be expected to contain no terminal liquid at the end of solidification. The Cu-Ni system is isomorphous, but does have a larger solidification temperature range than the Fe-Ni system for both equilibrium and non-equilibrium Scheil[19] solidification conditions. Scheil conditions are defined as equilibrium at the solid/liquid interface, no undercooling and negligible diffusion of solute in the solidifying solid. Because both binary systems are almost completely isomorphous, they are expected to have low solidification cracking susceptibility.

According to the Fe-Ni-Cu liquidus projection, the minimum temperature occurs in the pure Cu phase at 1085°C (Figure 18[42]). Under Scheil conditions the composition of the terminal liquid is expected to be enriched to a minimum in the system. As such, Cu is expected to be the terminal point in the ternary system if Scheil solidification conditions exist, thereby resulting in an enlarged solidification temperature range as compared to equilibrium solidification conditions.

The objective of this work is to determine the minimum Ni interlayer concentration necessary to produce crack free Fe-Ni-Cu compositionally graded deposits. In this study, Ni-Cu and Fe-Ni-Cu weld deposits were made using the Gas Tungsten Arc Weld (GTAW) process and examined for cracking. Cracking susceptibility of Fe-Ni-Cu deposits was quantified through microstructural analysis and explained through

solidification modeling. The results of this work will provide insight towards the development of a deposition process that can combine Cu and H-13 tool steel for the die industry and the manufacturing community as a whole.

2-2. Experimental Procedure

To represent the Fe-Ni-Cu ternary system, SAE 1013 Steel (bar), Ni 99 (wire), Ni 200 (bar) and deoxidized (DEOX) Cu (wire) were chosen as base and filler metal materials. This model system will simplify the analysis by reducing the number of trace alloying elements, while producing results representative of the solidification behavior of H-13, Ni and Cu. The compositions for the alloys used in this work are listed in Table III.

The current work only considers compositional effects on solidification cracking. Therefore, a Gas Tungsten Arc Weld (GTAW) system with a cold wire feed was used to produce bead on plate deposits. These deposits were at least an order of magnitude wider than those produced by direct metal deposition, thereby simplifying sample preparation and subsequent analysis, yet still representative of solidification under relatively high cooling rates.

A wide range of binary Ni-Cu compositions were also fabricated by depositing a single pass bead-on-plate deposit. The experimental setup is described in more detail by Banovic et.al.[20]. DEOX Cu (1.143 mm diameter) filler metal wire was deposited onto rolled Ni 200 plate that was 0.635 cm thick and cut to 2.54 cm width.

To produce Fe-Ni-Cu deposits, multiple bead-on-plate deposits were prepared one on top of the other to simulate the direct metal deposition process. The first layer consisted of Ni-99 (1.143 mm diameter) filler metal wire deposited onto SAE 1013 steel. A second

pass of Ni-99 was required to produce deposits with over 60 wt% Ni, and was deposited on top of the first bead of Ni. Subsequent layers of Cu were deposited on top of the Fe-Ni layer by using DEOX Cu. The composition of each pass was varied by changing the filler metal feed rate and the arc current. The GTAW processing parameters for each condition are given in Table IV. The shielding gas was commercially pure Ar.

Transverse cross sections of samples from each processing condition were prepared using standard metallographic techniques. Cu rich regions were revealed by etching with equal parts 30% Hydrogen Peroxide, concentrated Ammonia and distilled water. The Fe-Ni samples were pre-etched in 30% Nirtric/70% methanol followed by etching in a 35% aqueous solution of Sodium Metabisulfite to reveal cell boundaries.

Both bulk and point compositions were determined with an electron-probe microanalyzer (EPMA). A JEOL 733 Super Probe, equipped with wavelength dispersive spectrometers (WDS), was operated at an accelerating voltage of 20 kV and a probe current of 25 nA for bulk analysis. To minimize the excitation volume yet maintain sufficient overvoltage to generate Cu Kα x-rays, the accelerating voltage was reduced to 15 kV for point analysis. To measure the nominal composition of the deposits, three to six measurements were acquired on each deposit from an area approximately 2000 μm^2 per measurement. This area was large enough to average out variations in composition due to microsegregation and provide good statistical measurement of the nominal deposit composition. A phi(ρZ) correction method was utilized to convert X-ray counts to weight percentages[21]. Compositional data was normalized for weight percent Fe, Ni and Cu, which is reasonable given the maximum amount of trace elements present in any deposit is 1.36 wt%, according to wet chemical analysis of the raw material.

Quantitative image analysis (QIA) was used to perform area fraction measurements of the Cu rich phase, which were assumed equivalent to the volume fraction. Twenty fields of view were measured for each composition to provide good statistical confidence in the area fraction measurements.

2-3. Results

Figure 19 is a schematic of a transverse cross-section of one such multi layer deposit with an example of accompanying compositions of each layer plotted on the Fe-Ni-Cu ternary phase diagram. Ni filler metal is deposited on AISI 1013 Steel for the first two layers, which moves the composition of each deposit towards the Ni rich corner of the ternary. Subsequent layers were fabricated by using Cu filler metal wire, thereby increasing the Cu content of each layer and moving the composition towards the Cu rich corner. **Figure 20** is a summary of the solidification cracking results for the Fe-Ni-Cu deposits with results for the Fe-Cu system included from previous work (Section I). Solidification cracking was not observed in the binary Fe-Ni and Ni-Cu deposits, however, solidification cracks were observed in ternary Fe-Ni-Cu deposits even with an interlayer consisting of up to 75 wt% Nickel.

A comparison of **Figure 21** and **Figure 22**, light optical micrographs of Fe-2.5 Ni-17.0 Cu and Fe-13.2 Ni-15.5 Cu samples, respectively, provide insight into the cracking mechanism. Cracking is observed exclusively along Cu rich regions. Additionally increasing the Ni content with similar nominal Cu concentration results in the formation of less terminal Cu during solidification. The effects of Ni additions on the amount of terminal Cu rich phase for approximately constant nominal Cu concentrations (16.4 ± 0.7

wt% Cu and 13.3 ± 0.5 wt% Cu) is presented in **Figure 23**. The volume percent of Cu rich phase in Fe-Ni-Cu deposits with similar Cu concentration but changing Fe to Ni ratio are plotted. As expected, exchanging Ni for Fe reduces the amount of terminal Cu due to the increased solubility of Cu[37]. Conversely, an increase in Cu concentration with similar Fe-Ni ratio is expected to result in a greater amount of Cu rich phase. This can be seen in the light optical micrograph for the Fe-10.0 Ni-24.0 Cu deposit (**Figure 24**), which has 12.8 volume percent Cu, as compared to **Figure 22**, which has a similar Fe-Ni ratio, but a lower Cu concentration and only 4.7 volume percent Cu..

A change in morphology is observed when both Ni and Cu concentrations are increased. The resultant microstructure for an Fe-28.2 Ni-57.8 Cu alloy can be seen in Figure 25, where a distinct Cu rich phase is not observed. In this alloy, there is no distinct interface between what appears to be Cu rich and Fe-Ni regions. Figure 25 is representative of the second class of ternary microstructure and alludes to a change in solidification behavior, which will be discussed in the next section.

2-4. Discussion

2-4-1. Solidification Behavior

As has been shown for the Fe-Cu system (Section I), solidification behavior and the nominal composition control the solidification temperature range and amount of terminal liquid. Two key metallurgical factors to solidification cracking susceptibility are the solidification temperature range and amount of terminal liquid. To understand cracking susceptibility it is necessary to determine the solidification behavior, which is a function of the dimensionless back diffusion parameter, α[28]. Solidification behavior is bounded

by equilibrium and non-equilibrium (Scheil) conditions. The upper and lower bounds for the amount of terminal liquid and the solidification temperature range can be determined by these two solidification conditions.

It has been shown that microsegregation in welds is a function of the back diffusion potential of solute elements in the solidifying solid as the weld freezes[17,25-28]. Alloy systems with a small back diffusion potential will experience greater levels of microsegregation during solidification. The greater microsegregation will produce a larger amount of terminal solute rich liquid, which will impact the solidification cracking susceptibility of the alloys system.

To determine the solidification behavior of Fe – Ni – Cu alloys, and determine the amount of terminal Cu rich liquid that would form during solidification, the dimensionless back diffusion coefficient α must be calculated. Once the solidification behavior is known, the solidification temperature range and amount of terminal liquid can be determined.

In order to determine the solidification condition for the Fe-Ni-Cu ternary system, the dimensionless back diffusion parameter (α) was calculated for the three binary systems. If all three binary systems have negligible back diffusion potential, then it is reasonable to interpolate that the back diffusion potential for the entire Fe-Ni-Cu system is negligible as well. A detailed calculation of the back diffusion parameter can be found in a previous work (Section I). The essential elements of its calculation for the Fe-Ni-Cu system are given below.

The back diffusion potential for the Fe-Cu system was found to be negligible (α = 0.0054) (Section I). The back diffusion potential for the Fe-Ni and Ni-Cu samples were

found using Fe-24.0 Ni and Ni-15.5 Cu samples respectively. Following the Brody-Fleming[28] solidification model, α is a function of D_s, the diffusivity of the solute (Ni or Cu) in the solid (γ Fe or Ni), t_f, the solidification time, and L, the distance the solute must travel to eliminate any compositional gradient, which is half the dendrite arm width.

The solidification time, t_f, can be determined by calculating the solidification temperature range, ΔT and the cooling rate, assuming that the cooling rate is linear. The Rosenthal equation for three dimensional heat flow from a point heat source was used to estimate the cooling rate along the weld center line[30]. The thermal conductivity, λ, for Fe and Ni at 727°C is 0.326 and 0.718 W/(cm °C), respectively[6]. These values for thermal conductivity were used as the effective thermal conductivity over the respective solidification temperature ranges. The conditions used to make the deposits were, VI = 3250 W, S = 0.2 cm/s, η_a = .75 for the GTAW process[31], T_o = 25°C, and T = 1465°C and 1428°C (liquidus temperature) for Fe-Ni and Ni-Cu respectively. Given the above, the Rosenthal approximated cooling rate was found to be 349°C/s for Fe-Ni and 729°C/s for Ni-Cu. The maximum solidification temperature range for Fe-Ni and Ni-Cu was 25°C, 343°C, respectively. The resultant solidification time was 0.07 seconds and 0.5 seconds for Fe-Ni and Ni-Cu respectively.

Because diffusivity is dependant on temperature, the value of the back diffusion potential will change as the deposit cools. Therefore, an upper bound estimation is made for the back diffusion potential (α_{max}) of both Fe-Ni and Ni-Cu samples. If α_{max} is found to be << 1, then both alloys will solidify under non-equilibrium conditions regardless of temperature.

To provide an upper bound estimation for α, the diffusivities of Ni in γ Fe and Cu in Ni were calculated at the respective liquidus temperatures. Diffusivity of Ni in γ Fe at 1465°C and Cu in Ni at 1428°C was found to be 1.1 X 10^{-13} m^2/s and 1.23 X 10^{-12} m^2/s, respectively[43]. The dendrite arm spacing was measured to be 20.7 microns and 11.3 microns for Fe-Ni and Ni-Cu respectively. The resultant α_{max} for Fe-Ni and Ni-Cu is then 0.00007 and 0.02, both of which are << 1. Since α_{max}<< 1 for the three constitutive binary systems, the solidification conditions for ternary Fe-Ni-Cu alloys are expected to be close to non-equilibrium Scheil conditions.

2-4-2 Solidification modeling

The solidification temperature range and amount of terminal liquid are two key metallurgical factors in the solidification cracking susceptibility of an alloy. The advent of computational thermodynamic programs, such as Thermocalc[44-46], enables the calculation of these two parameters over a broad range of Fe-Ni-Cu compositions. The use of the Scheil module[47] provides a means for predicting these values even when the equilibrium partition coefficient (k) varies with temperature and composition. It is anticipated that k will vary in Fe-Ni-Cu ternary space given that it is not constant with varying temperature and compositions for the three associated binary diagrams.

Figure 26 graphically displays the results of solidification calculations performed by ThermoCalc for the Fe-Ni-Cu system. Composition was varied by 10 wt% per calculation. The solidification temperature range and weight fraction of terminal liquid (in parenthesis) were calculated for the Scheil solidification condition. It was possible to carry out these calculations over the majority of the Fe-Ni-Cu system, except towards the Cu rich region. Scheil data from previous work (Section I) was used to complete the Fe-

Cu binary results. From these results two observations can be made. First, a large solidification temperature range of over 150°C is present for nearly all ternary compositions with solidification temperature range increasing as the nominal composition of Cu decreases. Second, no terminal Cu rich liquid is predicted when Ni concentrations exceed 30%.

Two characteristic types of solidification sequences were revealed by the ThermoCalc Scheil calculations for the Fe-Ni-Cu system. The first sequence involved two face centered cubic (FCC) phases, one primary, the second terminal. This is shown in **Figure 27**; a plot of fraction solid vs. temperature for the Fe-10.0 Ni-24.0 Cu deposit. In this case, two distinct phases form, which is consistent with the microstructure for this sample in **Figure 24**, where the terminal (intercellular) phase is Cu and the cells are a Fe-Ni-Cu solid solution γ phase. The second type of solidification sequence resulted in only one FCC phase upon solidification. A representative figure that shows this behavior can be seen in **Figure 28**, which is a fraction solid vs. temperature plot for the Fe-28.2 Ni-57.8 Cu alloy. In this case, the microstructure does not show a distinct Cu rich phase, as shown in **Figure 25**.

To ensure that the trends predicted by Thermocalc for the Fe-Ni-Cu system are accurate, the calculations must be validated by experimental results. The first means of validation is comparing the Thermocalc predicted terminal Cu rich liquid and that measured in experimentally produced deposits. This comparison can only be made for deposits that exhibited a terminal Cu rich phase: i.e. for deposits with Ni concentration less than 30 wt%. In **Figure 23** the Thermocalc predicted amount of terminal liquid can be compared with the experimental results. Reasonable agreement is found between

calculated and measured values, giving support to the validation of the Thermocalc modeling.

Comparing the Thermocalc predicted composition of each phase as a function of fraction solid formed was the second means of validation. **Figure 29**a is a scanning electron microscope (SEM) image taken of a cell in the Fe-10.0 Ni- 24.0 Cu sample. EPMA data was taken across this cell, with the white dots caused by beam damage during EPMA measurement, which serves as a useful guide to the location of the point measurements. The white intercellular region in the SEM image is Cu rich, as shown by the EPMA data presented in **Figure 29**b. **Figure 29**b presents the EPMA data taken across the cell in **Figure 29**a along with Thermocalc Scheil module predicted composition of the solid as a function of fraction solid. The cell core, which constitutes the first solid to form in the cell, is taken as $f_S=0$ and the interdendritic region, where the Cu concentration peaks and solidification terminates, as $f_S=1$. **Figure 30** is a similar SEM image and EPMA line scan for the Fe-28.2 Ni-57.8 Cu alloy, which is expected to have only one solid phase with continuously varying concentration.

Differences between the Scheil calculated and experimentally measured concentrations are most likely the result of shifts in the phase boundary lines due to the effect of the trace elements that were not included in the calculation. Additionally, the EPMA's ability to accurately measure the Cu rich intercellular concentrations in **Figure 29** is limited by the x-ray excitation volume of a 15 kV beam, which is on the order of 1 micron; approximately the same size as the intercellular region. Given the capabilities of the EPMA, and the potential effect of trace elements, good agreement exists between the ThermoCalc modeling and measured compositions.

Microstructural development provides an additional means to verify the Thermocalc model results. There is a marked difference in the as-solidified microstructures of **Figure 24** and **Figure 25**, as a distinct Cu rich second phase is absent in the latter. A second phase is not anticipated to form in an isomorphous system, such as Ni-Cu, even under Scheil solidification conditions. In an isomorphous phase diagram, the liquidus and solidus lines converge at the end of solidification, as can be seen for Ni-Cu in **Figure 17**. Physically, this means that all the solute in the liquid is absorbed by the single solid phase, thereby preventing the formation of a terminal liquid.

Unlike a binary system, the liquidus and solidus lines in a ternary system follow a three dimensional surface. The direction of their motion is dictated by the partition coefficients of each element. As such, isopleths constructed from a ternary phase diagram are of little use since they are constrained to two dimensions. Thermocalc provides the capability to obtain compositional data for phases as a function of temperature. This data is derived from the composition of solid and liquid at any given temperature along the solidus and liquidus surfaces. This compositional data, obtained from the solidification pathway in three dimensions, can then be plotted in two dimensions (temperature and composition) to form "pseudo" solidus and liquidus lines. The shape of the liquidus and solidus lines can provide insight on phase formation during solidification.

Figure 31 and **Figure 32** display pseudo liquidus and solidus lines for Fe-10.0 Ni-24.0 Cu and Fe-28.2 Ni-57.8 Cu alloys, respectively. The shape of the Cu pseudo liquidus and solidus in the former alloy is of similar shape to the binary Fe-Cu liquidus and solidus lines. The composition of these lines drastically changes at 1135°C upon the

formation of the second phase, which is Cu rich. In the Fe-28.2 Ni-57.8 Cu the shape of the Ni and Cu liquidus and solidus lines are of similar shape to those observed in an isomporphous diagram. The solidus and liquidus lines intersect, thereby precluding the formation of a terminal phase.

2-4-3. Cracking Susceptibility

The ThermoCalc Scheil model prediction of phases that form during solidification are also corroberated by the expimentally observed microstructures. This provides additional evidence that the Thermocalc calculations are valid. As such, the solidification temperature range and terminal liquid data presented in **Figure 26** can be used to explain the solidification cracking of **Figure 20**. A large solidification temperature range exists with Fe-Cu, Ni-Cu and Fe-Ni-Cu alloys. Additionally, significant amounts of terminal Cu rich liquid are formed for Ni concentrations less than 30 wt%. The combination of these two factors controls the cracking susceptibility of Fe-Ni-Cu alloys with less than 30 wt% Cu.

Even when there is no terminal Cu (Ni concentrations > 30 wt%), due to solidification as a single phase, there remains a large solidification temperature range of 250°C or greater in ternary alloys that crack. However, binary Ni-Cu alloys with similar solidification temperature range and absence of terminal liquid do not crack. This indicates that factors other than composition, which effects solidification temperature range and the amount of terminal liquid, play a significant role in the solidification cracking susceptibility of Fe-Ni-Cu alloys. Zacharia[48] has shown that stress distribution around the melt pool can have a significant effect on solidification cracking susceptibility. The heat flow, thermal stresses and solidification shrinkage are

mechanical factors that may play a significant role in the solidification cracking susceptibility of Fe-Ni-Cu deposits. It can be concluded that the concentration of the Ni interlayer must be greater than 75 wt% Ni to produce a compositionally graded deposit of Steel, Ni and Cu that is free of solidification cracking.

2-5. Conclusion

To determine the compositional cracking susceptibility of the Fe-Ni-Cu system, a wide range of Fe – Ni – Cu deposits was fabricated by GTAW with a cold wire feed. EPMA measurements were carried out to determine the composition of the deposits. Solidification cracking was observed when Cu was deposited onto Fe-Ni with Ni concentration of up to 75 wt% Ni.

The Thermocalc Scheil model was validated for the Fe-Ni-Cu system by comparison with experimental results, which showed good agreement with the Scheil calculations. Thermocalc Scheil calculations predicted a solidification temperature range of more than 150°C for nearly the entire ternary under Scheil solidification behavior.

Additionally, alloys with less than approximately 30 wt% Ni solidified as two FCC phases, whereas alloys with more than 30 wt% Ni were found to solidify as a single FCC phase. The solidification temperature range and amount of terminal liquid, which are effected by alloy composition, proved insufficient to fully explain solidification cracking susceptibility in the Fe-Ni-Cu system.

To produce functionally graded deposit of Steel, Ni and Cu that is free of solidification cracks, the concentration of the Ni interlayer must be greater than 75 wt%.

2-6. Individual Tables

Table III: Material Compositions in wt%

	C	Mn	Si	S	P	Cr	Ni	Mo	Cu	Fe	Al	Sn	Ti
Cu wire	-	0.18	0.23	-	0.01	-	-	-	98.78	-	-	0.8	-
Ni 99 wire	0.03	-	0.12	0.001	0.004	-	99.8	-	-	0.053	0.001	-	0.002
SAE 1013 Bar	0.13	0.82	0.173	0.02	0.007	0.026	0.066	0.015	0.08	98.643	0.009	0.011	-
Ni 200 bar	0.04	0.18	0.03	0.001	-	-	99.7	-	0.01	0.05	-	-	-

Table IV: GTAW Processing Parameters

Material	Arc gap (mm)	Travel speed (mm/s)	Arc potential (volts)	Arc current (amperes)	Wire feed speed (mm/s)
Cu* onto Ni99	2.54	2	10	325 to 130	8 to 45
Ni* onto 1013	2.54	2	10	375 to 325	4 to 71
Cu* onto Fe-Ni	2.54	2	10	200 to 125	4 to 25

2-7. Figures

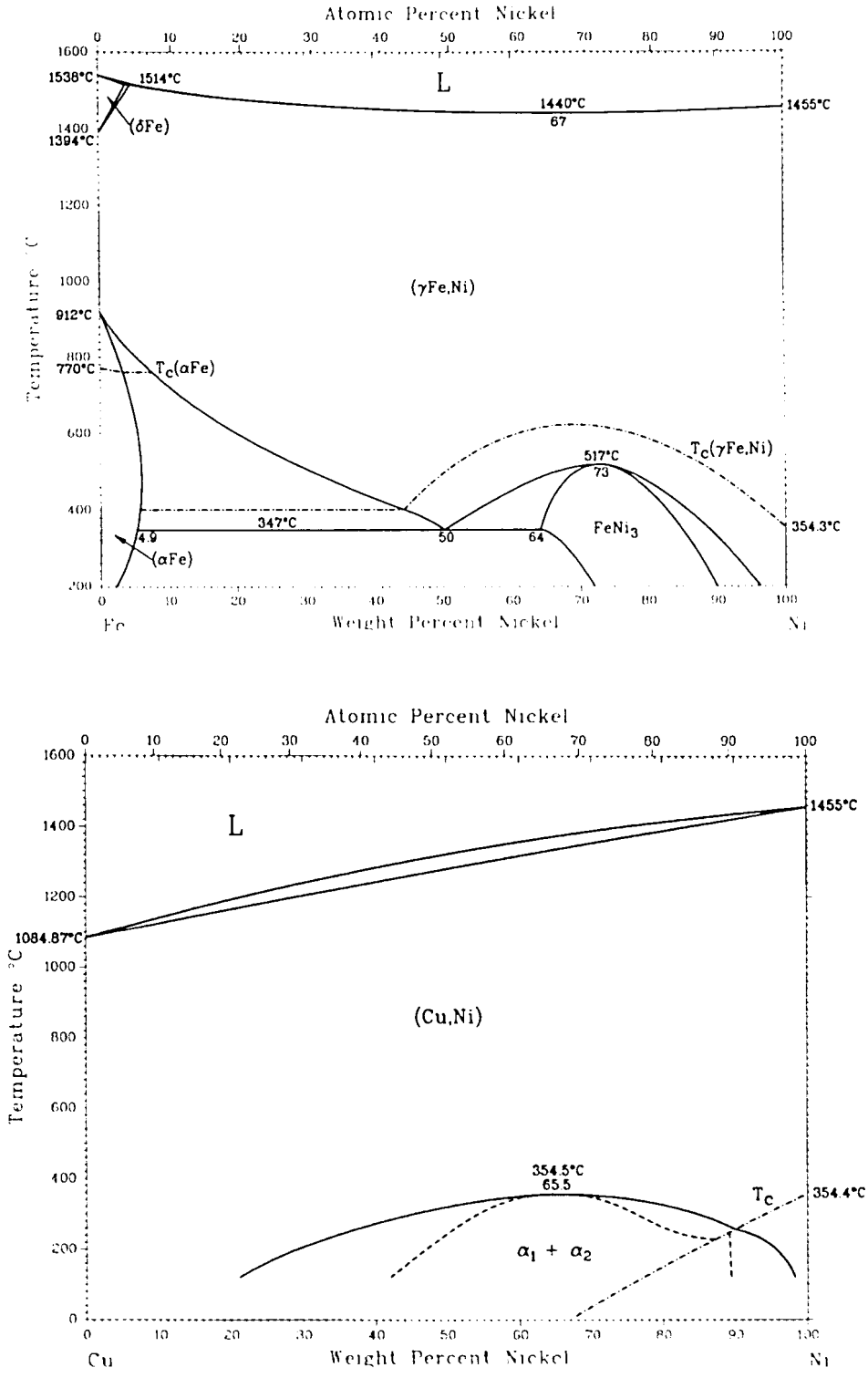

Figure 17: Phase diagrams[41] for a) Fe-Ni and b) Cu-Ni.

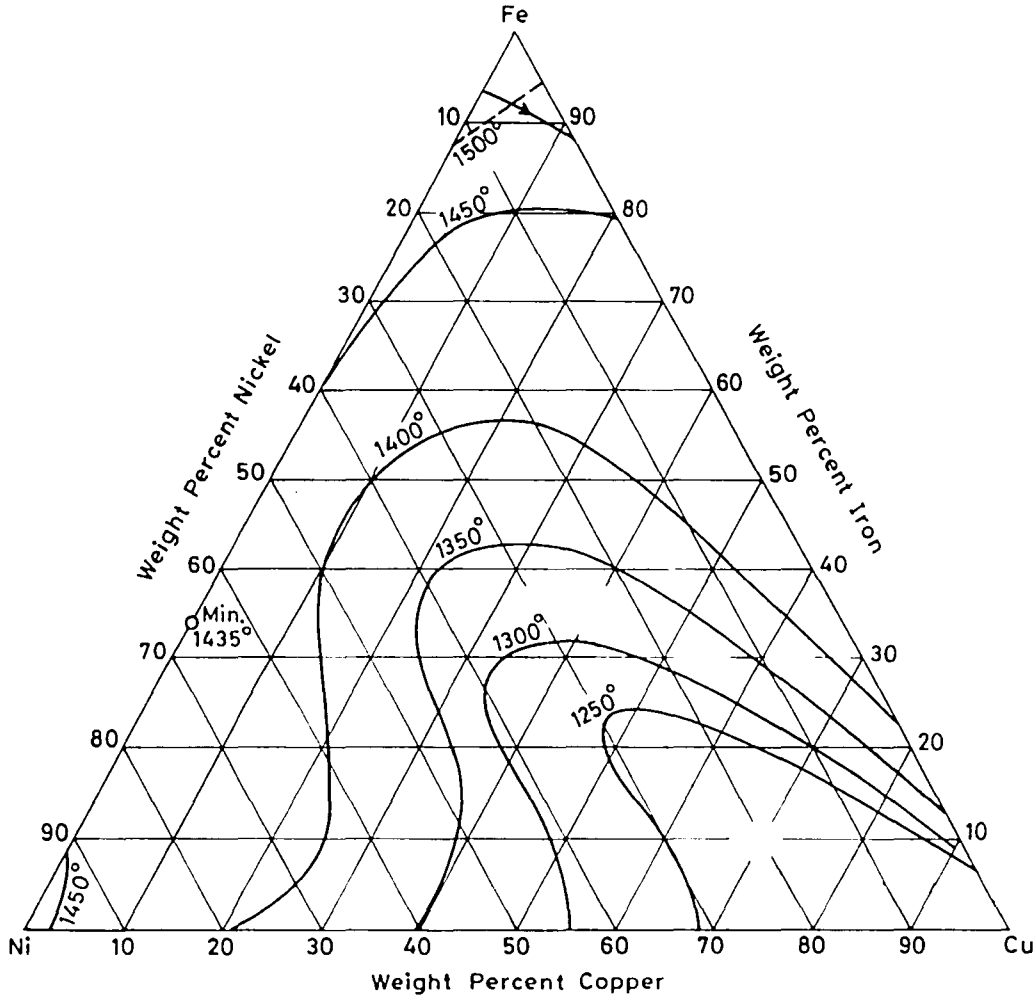

Figure 18: Fe-Ni-Cu liquidus projection[42].

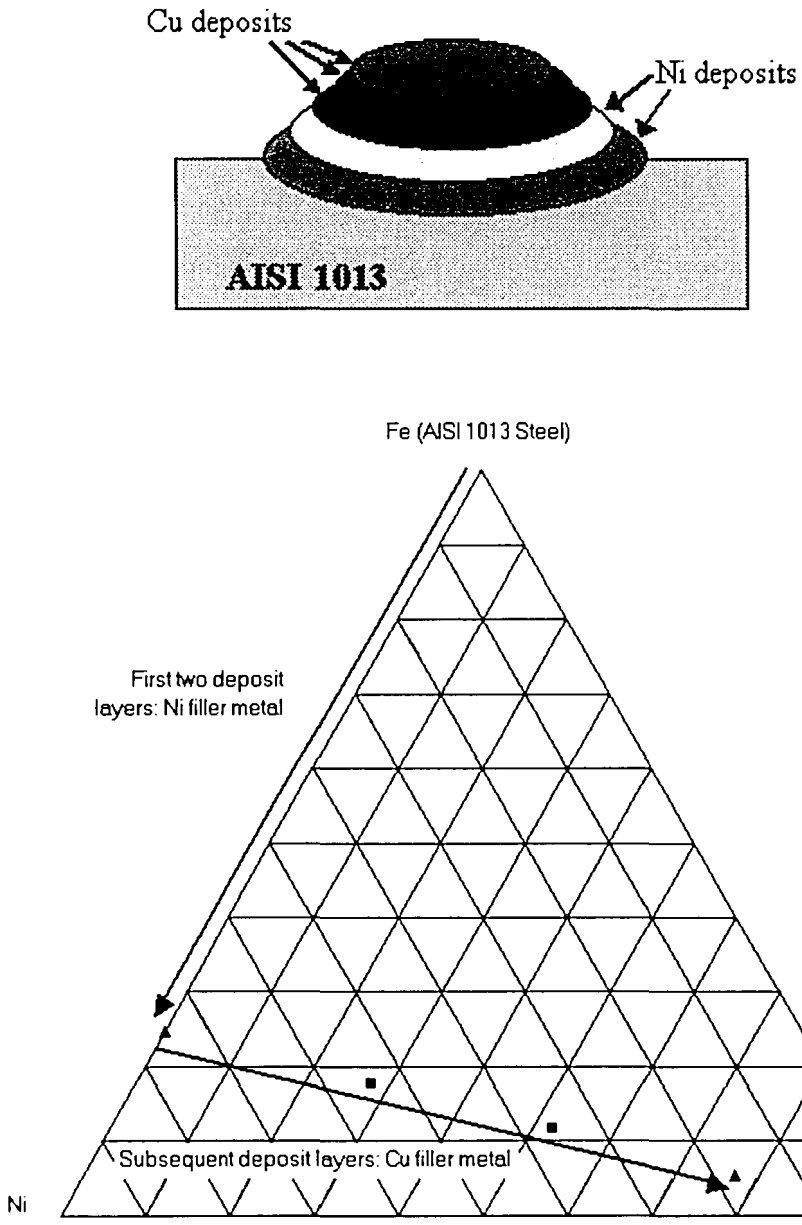

Figure 19: a) Schema of multi pass Fe-Ni-Cu deposits and b) resultant compositions of each layer plotted on Fe-Ni-Cu ternary diagram

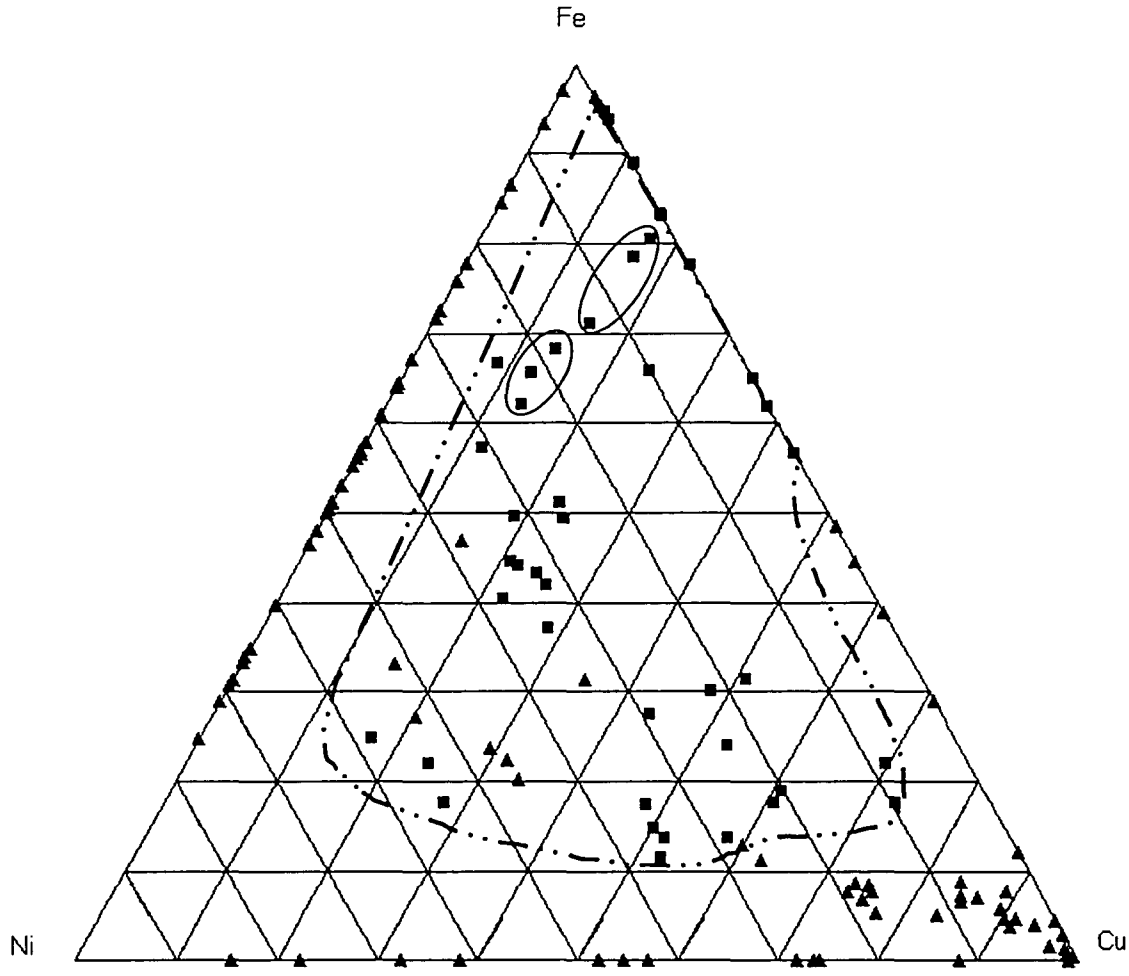

Figure 20: Solidification Cracking Results. Squares and triangles represent cracked and crack free compositions respectively. Dotted line defines crack susceptible composition range. Volume percent Cu rich phase for encircled data points displayed in Figure 23.

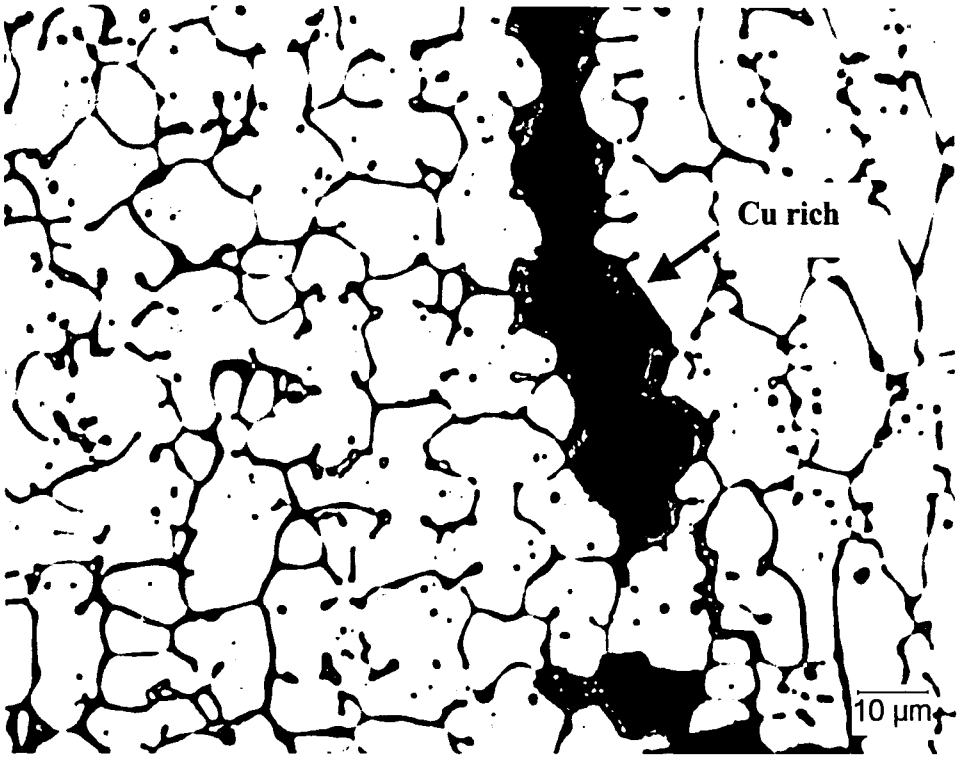

Figure 21: Fe-2.5Ni-17.0 Cu. Cracking observed along Cu rich regions.

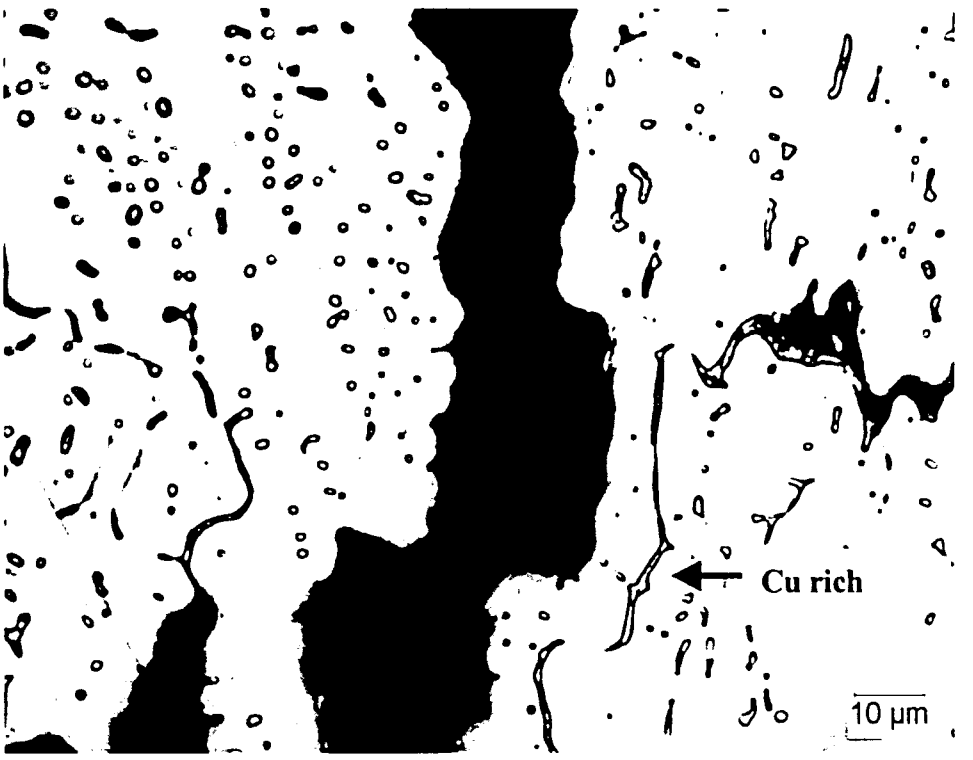

Figure 22: Fe-13.2Ni-15.5Cu. Cracking along Cu rich regions. Increased Ni results in less terminal Cu compared to Figure 21.

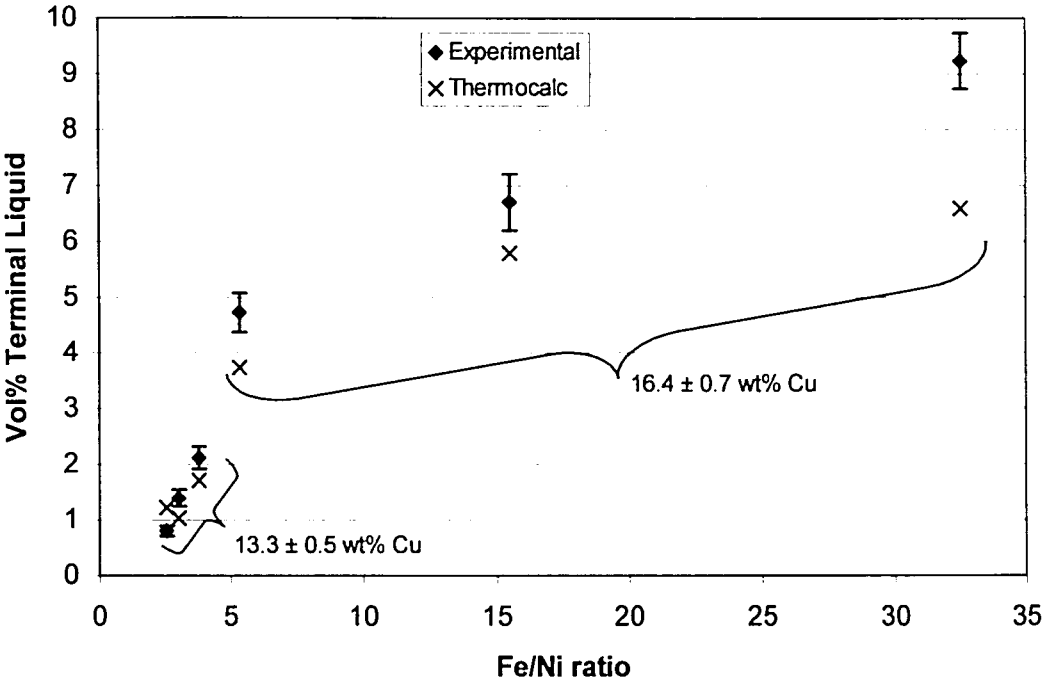

Figure 23: Effect of Ni concentration on Cu rich phase in Fe-Ni-Cu alloys.

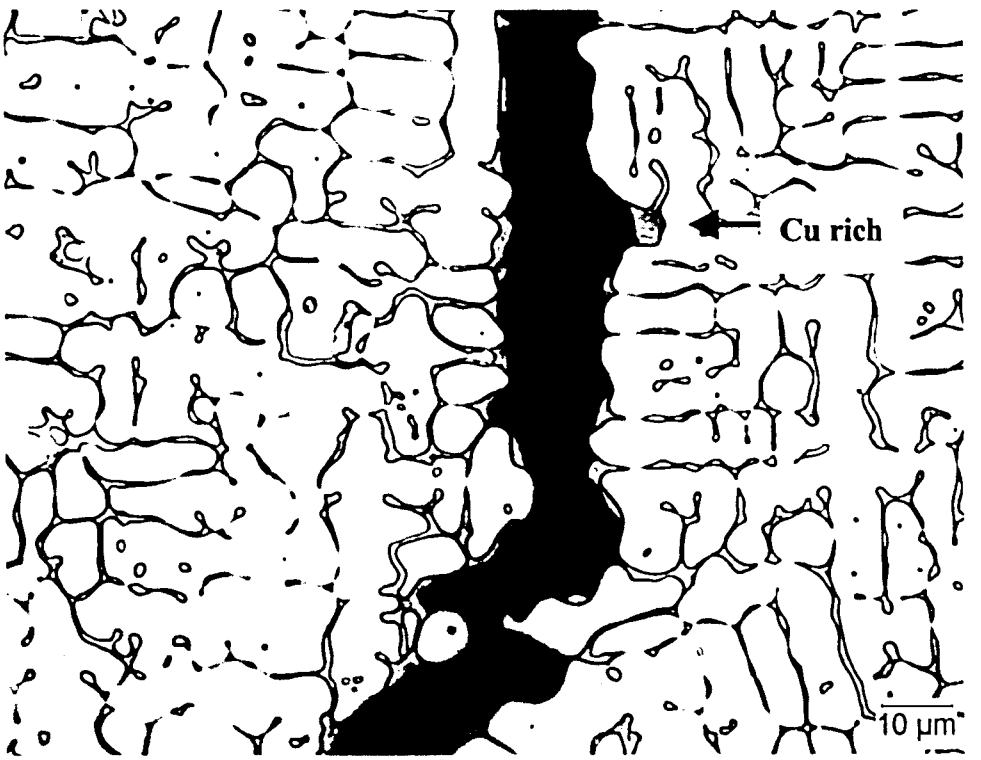

Figure 24: Fe-10.0Ni-24Cu deposit exhibiting cracking along Cu rich phase, but reduced amount of this phase as compared to Figure 22, which has similar Ni content but less Cu.

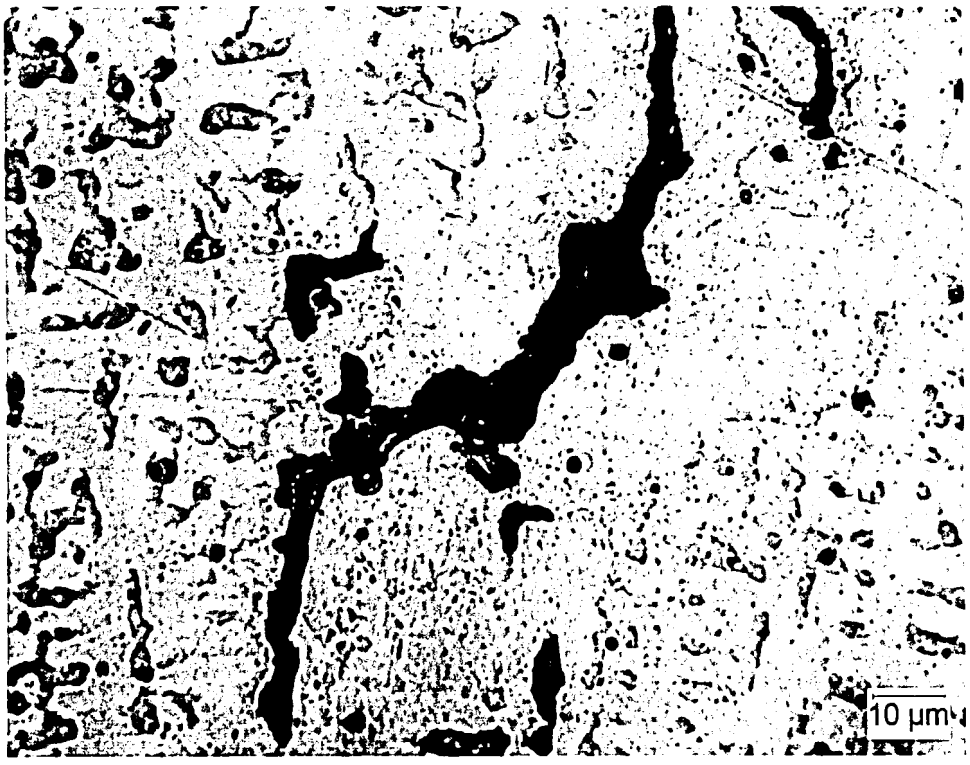

Figure 25: Fe-28.2Ni-57.8Cu deposit. Cracking is observed along Cu rich regions, however, a distinct Cu rich phase is no longer observed

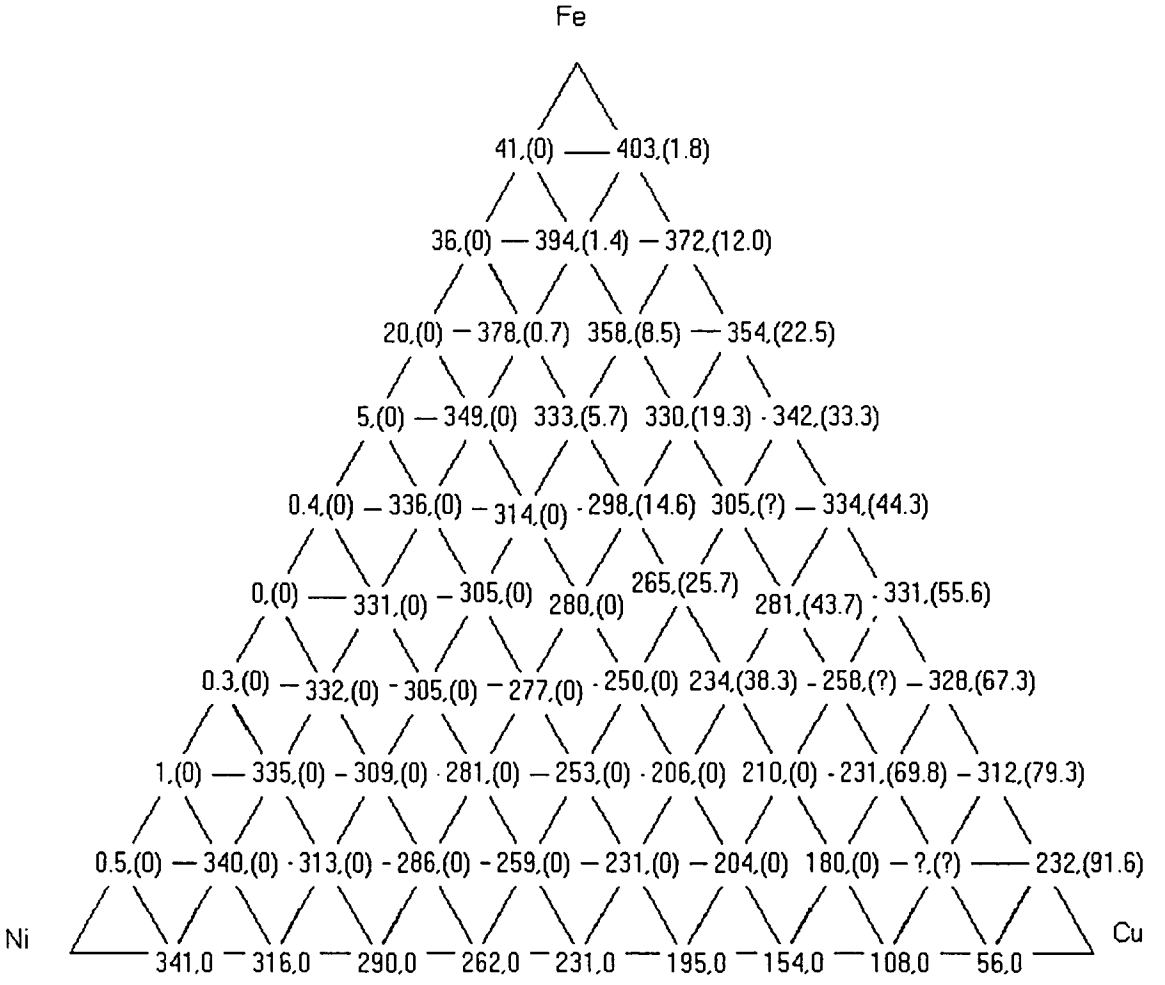

Figure 26: Solidification temperature range (C) and volume percent terminal Cu (in parenthesis) results from ThermoCalc Scheil module calculations

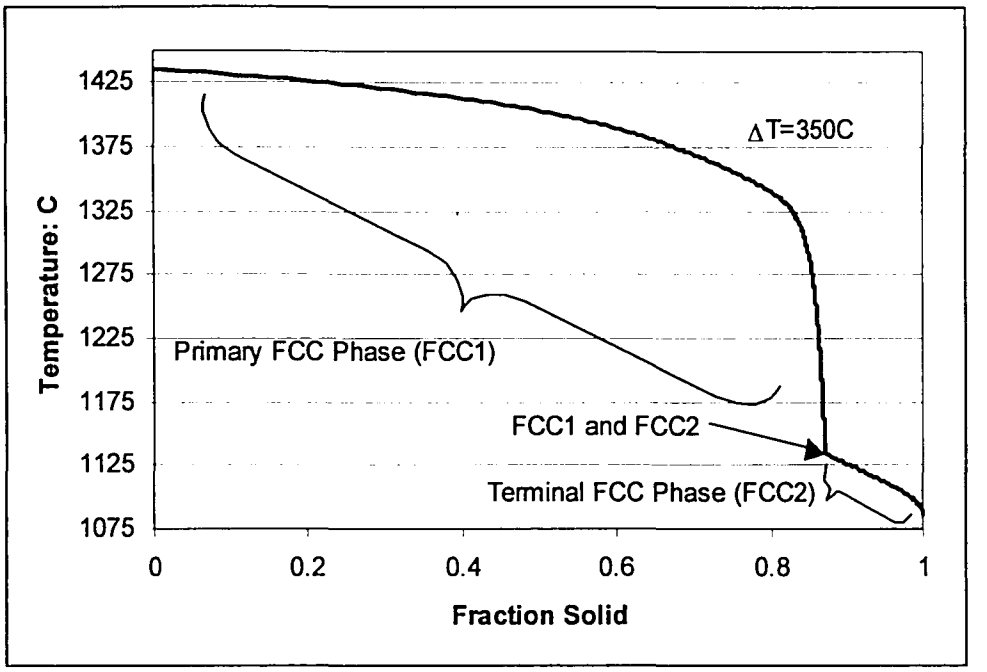

Figure 27: Thermocalc Scheil module predicted fraction solid vs temperature with solidified phases for Fe-10.0 Ni-24.0 Cu. Solidifies as two FCC phases, one primary and one terminal.

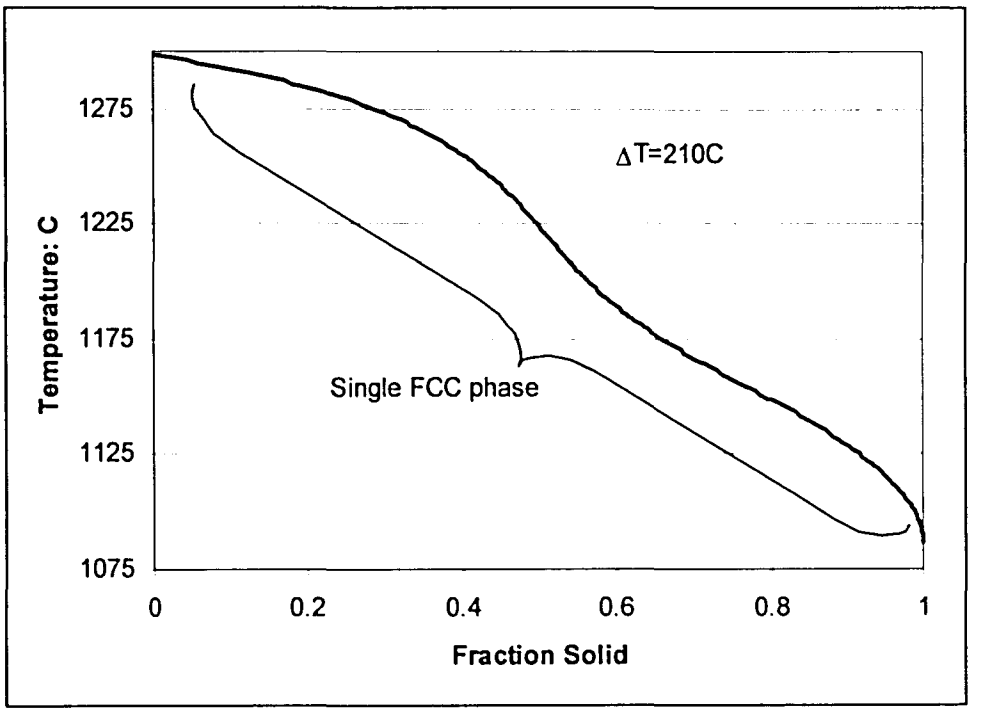

Figure 28: Thermocalc Scheil module predicted fraction solid vs temperature with solidified phase designations for Fe-28.2 Ni- 57.8 Cu. Solidifies as a single FCC phase.

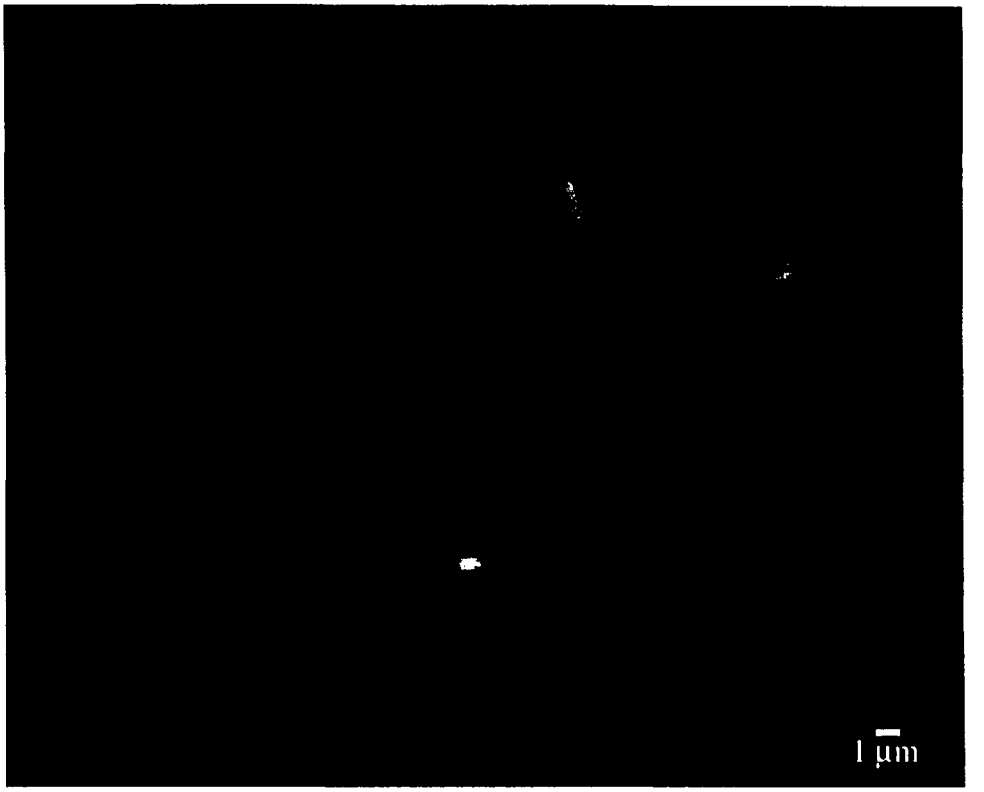

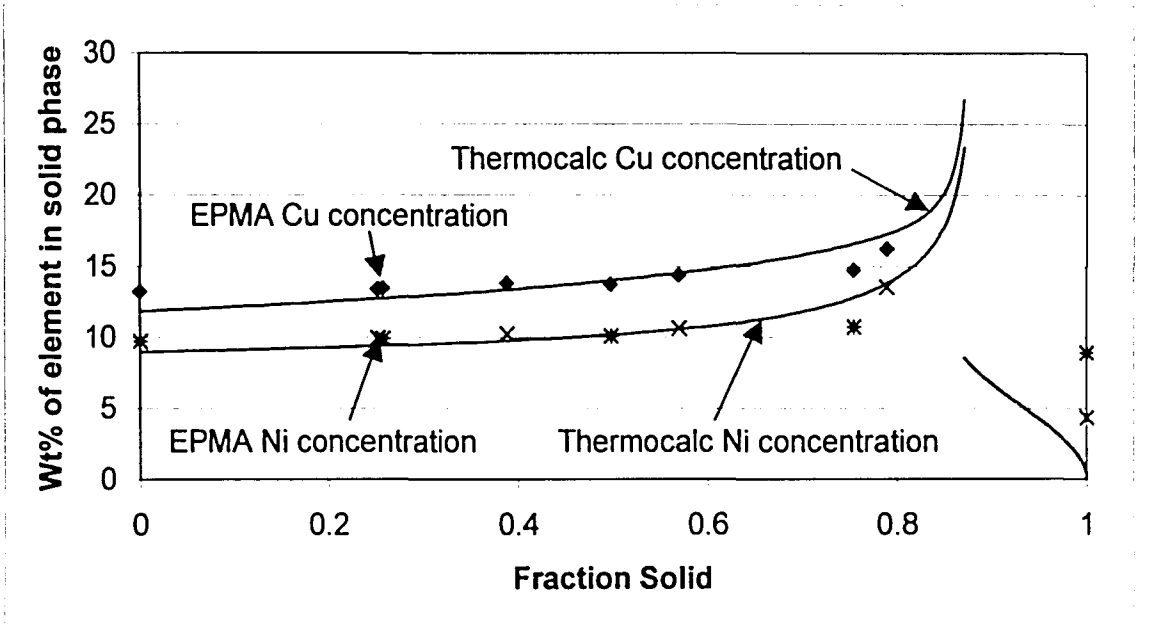

Figure 29: a) SEM micrograph of EPMA line scan on Fe-10.0 Ni- 24.0 Cu. White dots are beam damage and indicate where compositional data was collected b) EPMA data and Thermocalc predicted concentration as a function of fraction solid formed.

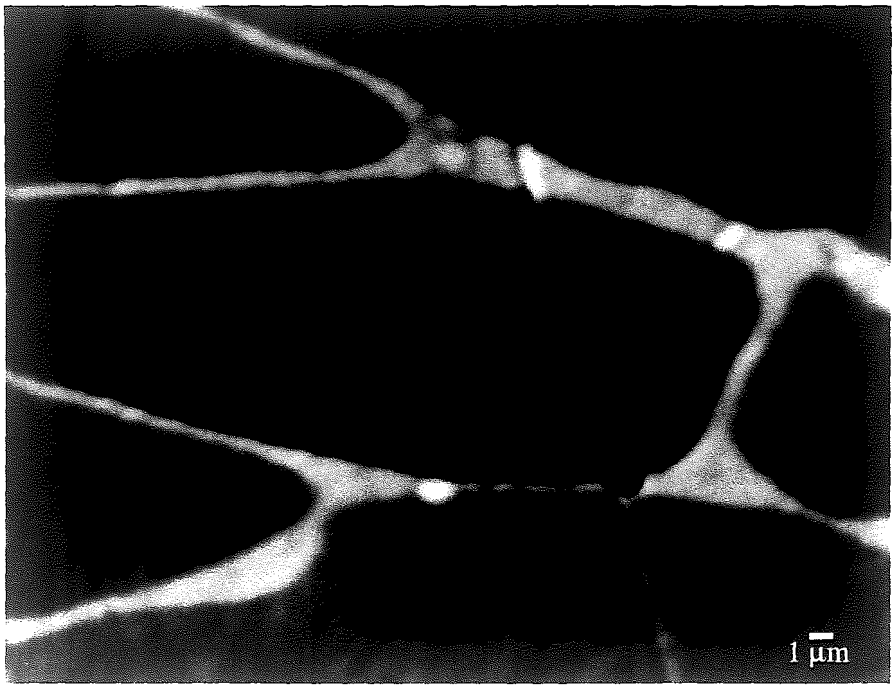

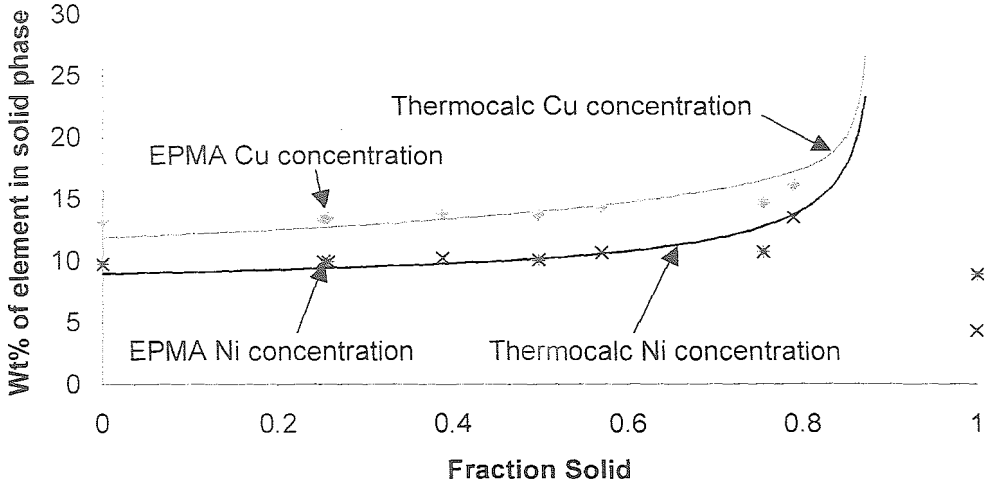

Figure 29: a) SEM micrograph of EPMA line scan on Fe-10.0 Ni- 24.0 Cu. White dots are beam damage and indicate where compositional data was collected b) EPMA data and Thermocalc predicted concentration as a function of fraction solid formed.

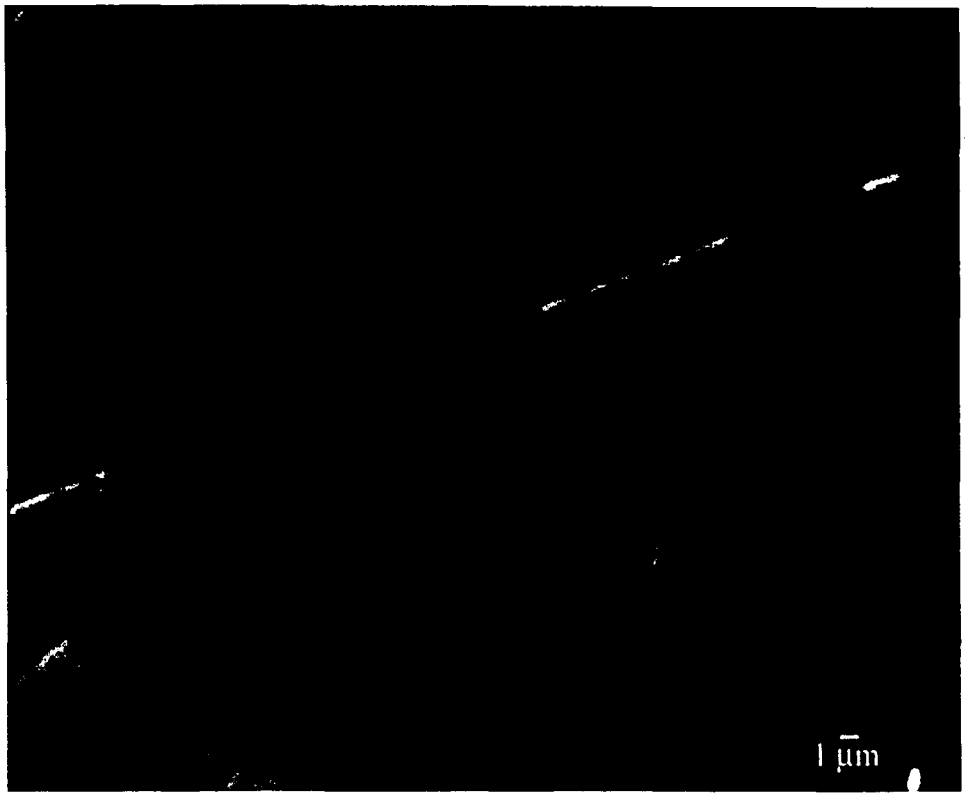

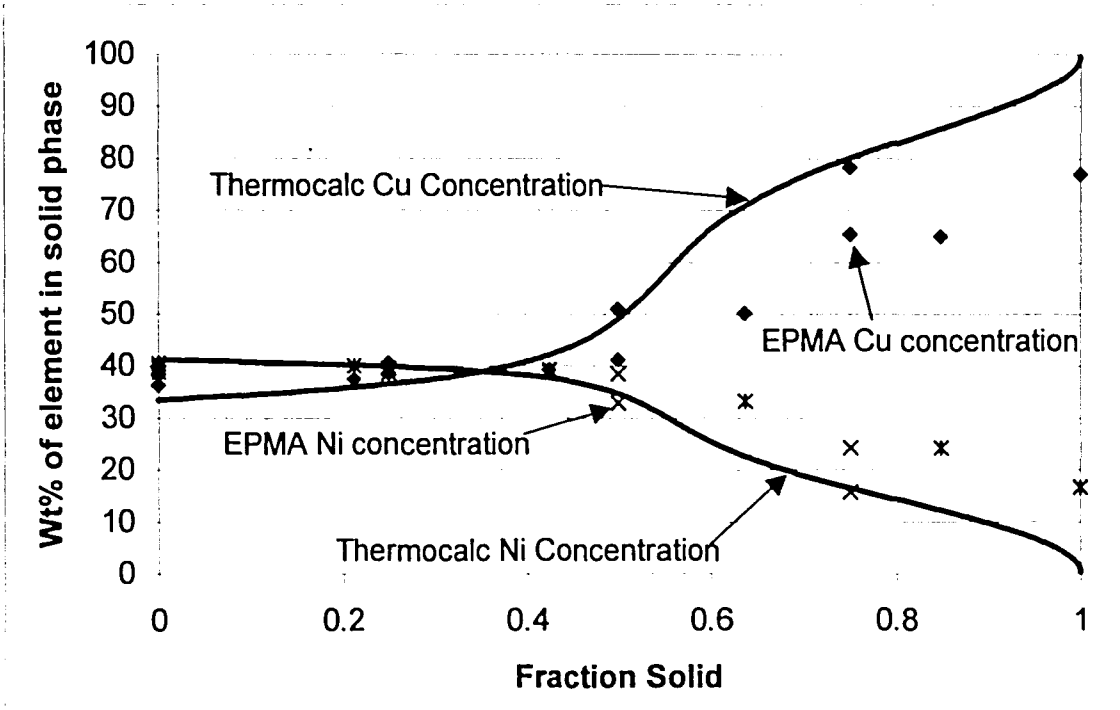

Figure 30: a) SEM micrograph of EPMA line scan on Fe-28.2 Ni- 57.8 Cu. White dots are beam damage and indicate where compositional data was collected b) EPMA data and Thermocalc predicted concentration as a function of fraction solid formed.

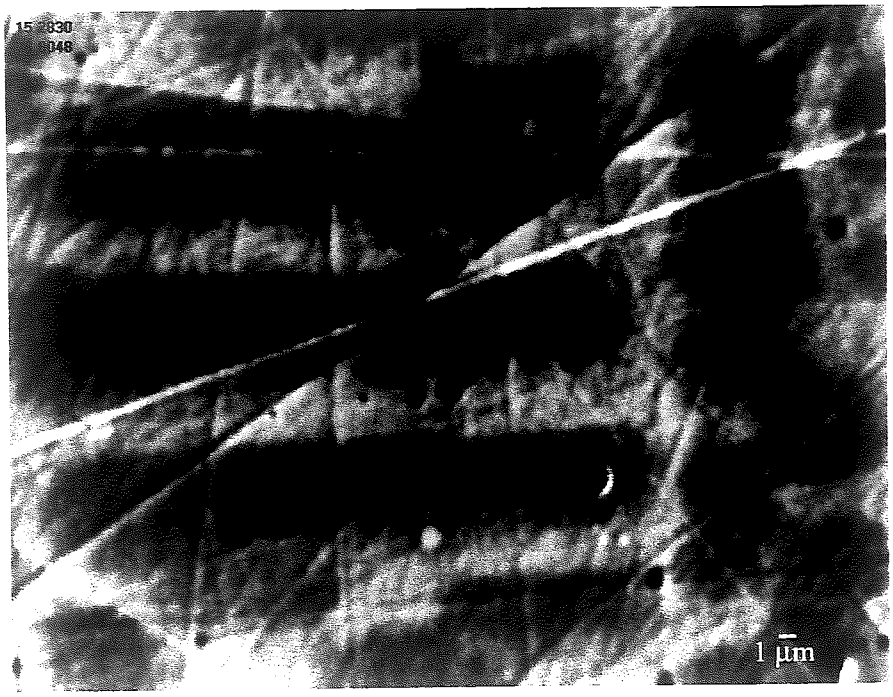

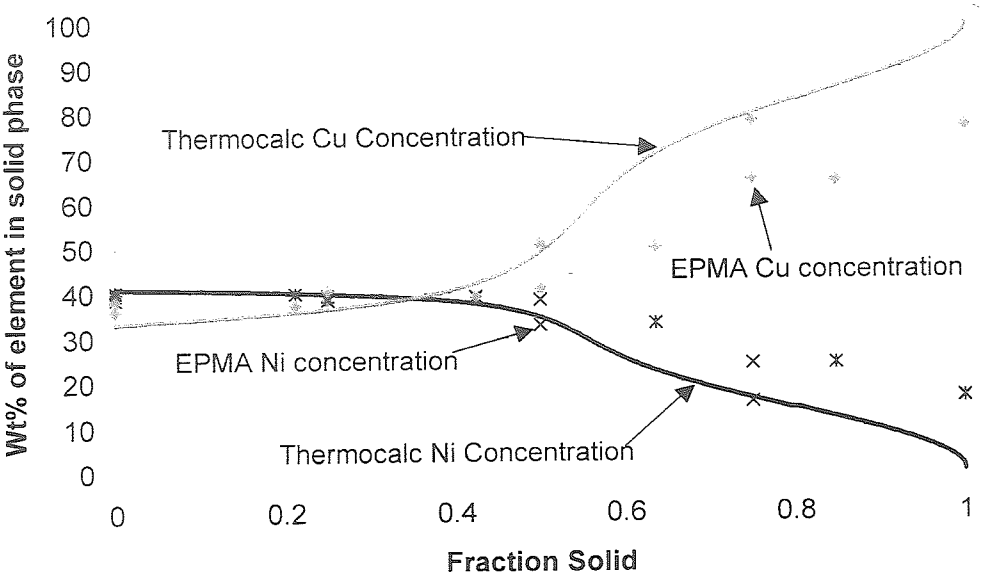

Figure 30: a) SEM micrograph of EPMA line scan on Fe-28.2 Ni- 57.8 Cu. White dots are beam damage and indicate where compositional data was collected b) EPMA data and Thermocalc predicted concentration as a function of fraction solid formed.

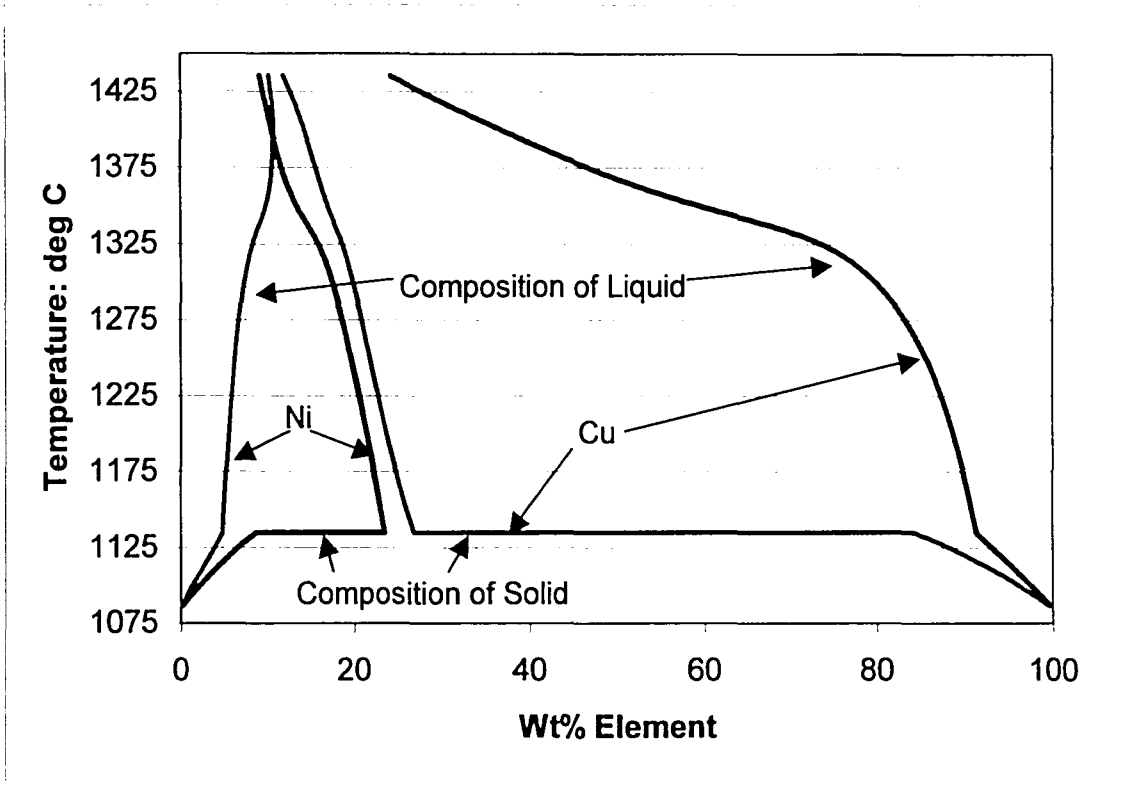

Figure 31: Pseudo solidus and liquidus lines for Ni and Cu in Fe-10.0 Ni-24.0 Cu alloy

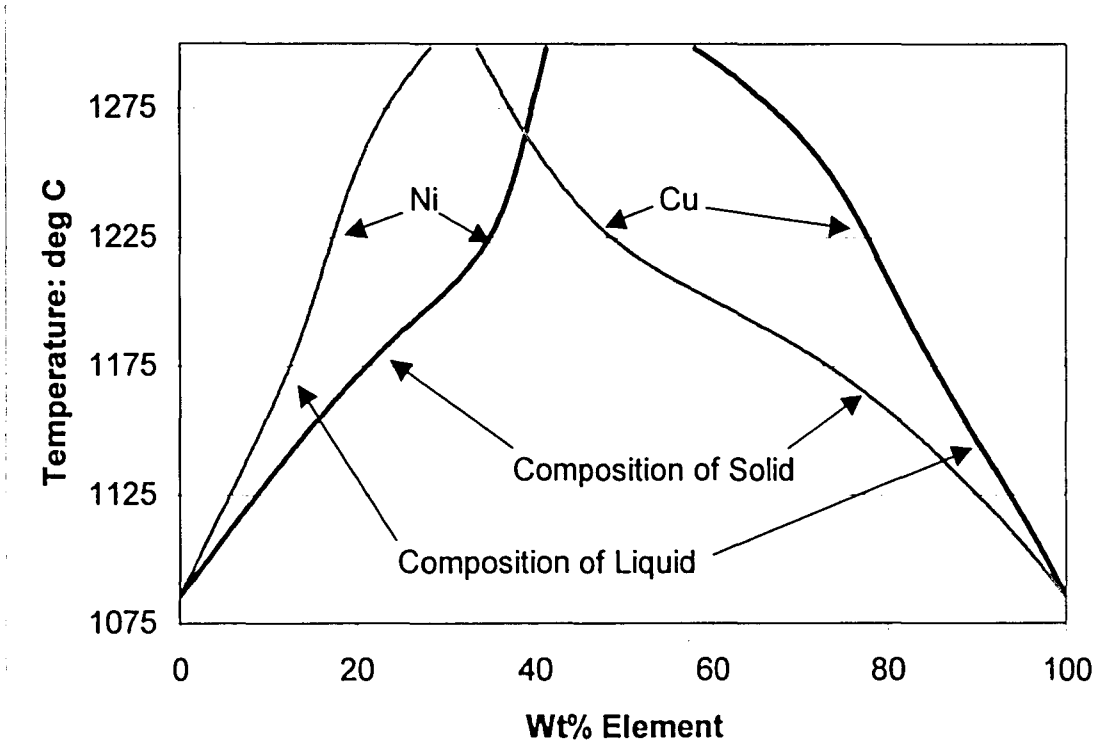

Figure 32: Pseudo solidus and liquidus lines for Ni and Cu in Fe-28.2 Ni-57.8 Cu

Reference List

1. J. Mazumder, J. Choi, K. Nagarathnam, J. Koch, and D. Hetzner, The direct metal deposition of H13 tool steel for 3-D components. *JOM* **49**, 55-60 (1997).

2. Knights, Rapid Tooling is Ready for Prime Time. *Plastics Technology (USA)* **47**, 46-53 (2001).

3. W. Liu and J. N. DuPont, Fabrication of functionally graded TiC/Ti composites by laser engineered net shaping. *Scripta Materialia* **48**, 1337-1342 (2003).

4. X. C. Li, J. Stampfl, and F. B. Prinz, Mechanical and thermal expansion behavior of laser deposited metal matrix composites of Invar and TiC. *Materials Science & Engineering, A: Structural Materials: Properties, Microstructure and Processing* **A282**, 86-90 (2000).

5. C. A. Brice, K. I. Schwendner, S. Amancherla, H. L. Fraser, and X. D. Zhang, Characterization of laser deposited niobium and molybdenum silicides. *Materials Research Society Symposium Proceedings* **625**, 31-35 (2000).

6. Y. S. Touloukian, *Thermophysical Properties of Matter Volume 1: Thermal Conductivity*, IFI/Plenum, New York, Washington (1970).

7. Alloy Data: No. 883 (AISI H-13) Tool Steel. 2003.

8. P. Engelmann, E. Dawkins, J. Shoemaker, and M. Monfore, Improved product quality and cycle times using copper alloy mold cores. *Journal of Injection Molding Technology* **1**, 18-24 (1997).

9. F. F. Noecker, II and J. N. DuPont. Functionally graded copper-steel using lens process. 2002. Rapid Prototyping of Materials, Proceedings of [a] Symposium, Columbus, OH, United States, Oct. 7-10, 2002.
Ref Type: Conference Proceeding

10. E. A. Asnis and V. M. Prokhorenko, Mechanism of cracking during the welding or depositing of copper on to steel. *Welding Production* **12**, 15-17 (1965).

11. A. E. VAINERMAN and A. A. OSETNIK, The Formation Of Cracks During The Deposition Of Copper Alloys On Steel. *Automated Welding* **21**, 22-25 (1968).

12. R. B. Cooper and T. H. Burns, How copper and sulfur influence hot cracking of carbon steel. *Metals Engineering Quarterly* **14**, 41-44 (1974).

13. B. Dixon, Weld metal solidification cracking in ferritic steels - a review. *Aust. Weld. J.* **26**, 23-30 (1981).

14. J. C. Borland, Fundamentals Of Solidification Cracking In Welds. Part 1. *WELDING AND METAL FABRICATION* **47**, 19-29 (1979).

15. J. C. Borland, Fundamentals Of Solidification Cracking In Welds. Part 2. *WELDING AND METAL FABRICATION* **47**, 99-107 (1979).

16. Y. Arata, F. Matsuda, and S. Katayama, Solidification crack susceptibility in weld metals of fully austenitic stainless steels. II. Effect of ferrite, phosphorus, sulfur, carbon, silicon, and manganese on ductility properties of solidification brittleness. *Transactions of JWRI* **6**, 105-116 (1977).

17. J. A. Brooks. Weld microsegregation: modeling and segregation effects on weld performance. 1990. Weldability Mater., Proc. Mater. Weldability Symp.

18. L. J. Swartzendruber, Cu-Fe. In *Binary Alloy Phases Diagrams: Second Edition, Volume 2* ed. by T. B. Massaiski, pp 1408-1410. ASM International, Ohio (1990).

19. E. Scheil, Bemerkungen zur Schichtkristallbildung. *Zeitschrift fur Metallkunde* **34/35**, 70-72 (1942).

20. S. W. Banovic, J. N. DuPont, and A. R. Marder, Dilution control in gas-tungsten-arc welds involving superaustenitic stainless steels and nickel-based alloys. *Metallurgical and Materials Transactions B: Process Metallurgy and Materials Processing Science* **32B**, 1171-1176 (2001).

21. J. I. Goldstein, D. E. Newbury, P. Echlin, D. C. Joy, A. D. Romig, C. E. Lyman, C. Fiori, and E. Lifshin, *Scanning Electron Microscopy and X-Ray Microanalysis*, Plenum, New York and London (1992).

22. D. W. Zeng, C. S. Xie, and K. C. Yung, Mesostructured composite coating on SAE 1045 carbon steel synthesized in situ by laser surface alloying. *Materials Letters* **56**. 680-684 (2002).

23. S. P. Elder, A. Munitz, and G. J. Abbaschian, Metastable liquid immiscibility in iron-copper and cobalt-copper alloys. *Materials Science Forum* **50**, 137-150 (1989).

24. A. Munitz, Liquid separation effects in Fe-Cu alloys solidified under different cooling rates. *Metallurgical Transactions B: Process Metallurgy* **18B**, 565-575 (1987).

25. J. N. DuPont, Microstructural development and solidification cracking susceptibility of a stabilized stainless steel. *Welding Research (Miami)* 253S-263S (1999).

26. J. N. DuPont, Solidification of an alloy 625 weld overlay. *Metallurgical and Materials Transactions A: Physical Metallurgy and Materials Science* **27A**, 3612-3620 (1996).

27. T. W. Clyne, M. Wolf, and W. Kurz, The effect of melt composition on solidification cracking of steel, with particular reference to continuous casting. *Metallurgical Transactions B: Process Metallurgy* **13B**, 259-266 (1982).

28. H. D. Brody and M. C. Flemings, Solute redistribution in dendritic solidification. *Trans. Met. Soc. AIME* **236**, 615-624 (1966).

29. M. Arita, M. Tanaka, K. S. Goto, and M. Someno, Activity and diffusivity measurements of copper in .gamma. and .delta. Fe by equilibration between solid iron and liquid silver. *Metall. Trans. , A* **12** , 497-504 (1981).

30. D. Rosenthal. The Theory of Moving Sources of Heat and Its Application to Metal Treatments. Transactions of A.S.M.E. 68, 849-866. 1946.

31. J. N. DuPont and A. R. Marder. A comparative study on the arc and melting efficiencies of arc welding processes. 1996. Trends in Welding Research, Proceedings of the International Conference, 4th, Gatlinburg, Tenn., June 5-8, 1995.

32. J. A. Brooks and M. I. Baskes. Weld microsegregation characterization and modeling. 1986. Adv. Weld. Sci. Technol., Proc. Int. Conf. Trends Weld. Res.

33. L. J. Swartzendruber, Cu-Fe (Copper-Iron). In *Phase Diagrams of Binary Copper Alloys* ed. by P. R. Subramanian, D. J. Chakraborit, and D. E. Laughlin, pp 167-172. ASM International, Materials Park (1994).

34. Y. Nakagawa, Liquid immiscibility in copper-iron and copper-cobalt systems in the supercooled state. *Acta Met.* **6**, 704-711 (1958).

35. Q. Chen and Z. Jin, The Fe-Cu system: a thermodynamic evaluation . *Metallurgical and Materials Transactions A: Physical Metallurgy and Materials Science* **26A**, 417-426 (1995).

36. D. W. Zeng. 2002.

37. W. J. M. Salter, Effects of alloying elements on solubility and surface energy of copper in mild steel. *J. Iron Steel Inst. (London)* **204**, 473-483 (1966).

38. K. P. Rao and A. Periyasamy, Hot cracking tendency of claddings of copper, nickel, and their alloys. *Prakt. Metallogr.* **29**, 564-572 (1992).

39. E. F. Nippes and D. J. Ball, Copper-contamination cracking: cracking mechanism and crack inhibitors. *Weld. Res. (Miami)* 75-81 (1982).

40. M. M. Borisenko, N. M. Novozhilov, A. I. Oldakovskii, and K. V. Bagryanskii, Effect of copper and nickel on some properties of weld metal. *Svar. Proizvod.* 29-30 (1975).

41. T. B. Massalski, *Binary Alloy Phase Diagrams*, ASM International, Materials Park, Ohio (1990).

42. K. P. Gupta, The Cu-Fe-Ni System. In *Phase Diagrams of Ternary Nickel Alloys*pp 290-315. Indian Institute of Metals, Calcutta (1990).

43. E. A. Brandes, Diffusion in Metals. In *Smithells metals reference book*, 7th Edn,pp 23. Butterworth-Heinemann, Oxford, Boston (1992).

44. B. Sundman, Review of Alloys Modelling. *Anales de Fisica, Serie B* **86**, 69-82 (1990).

45. B. Sundman, B. Jansson, and J. O. Andersson, The Thermo-Calc databank system. *CALPHAD: Computer Coupling of Phase Diagrams and Thermochemistry* **9**, 153-190 (1985).

46. J. O. Andersson, T. Helander, L. Hoglund, P. Shi, and B. Sundman, Thermo-Calc & DICTRA, computational tools for materials science. *CALPHAD: Computer Coupling of Phase Diagrams and Thermochemistry* **26**, 273-312 (2002).

47. B. Jansson, M. Schalin, M. Selleby, and B. Sundman. The Thermo-Calc database system. 1993. Comput. Software Chem. Extr. Metall., Proc. Int. Symp., 2nd .

48. T. Zacharia, Dynamic stresses in weld metal hot cracking. *Welding Research (Miami, FL, United States)* 164/S-172/S (1994).

Vita

Rick was born on 3 April, 1974 in Reading PA to his parents, Fred (Fredrick) and Georgia Noecker. He was raised in Reading PA and its surrounding suburbs, eventually attending Exeter Township Senior High School where he played varsity soccer and basketball. In June 1992 he graduated in the top 10% of his high school class and became an Air Force ROTC cadet at Lehigh University's Detachment 715.

As a cadet, he had several successes, to include earning the Distinguished Graduate award at AFROTC Field Training (ROTC "boot camp") during the summer of 1993. Additionally, Rick was the last cadet unit commander at Detachment 715, which closed in June 1995. He was also very active in student leadership on campus. He was a Gryphon (Resident Assistant) for three years. As a Gryphon, he received two distinguished awards: the "Intervener of the Year", awarded during his Junior year and "Gryphon of the Year", which he received at the culmination of his Senior year.

In June 1996, Rick graduated from Lehigh with honors and was the recipient of the Dr. Cyril John Osborn Award. He was commissioned a 2Lt Noecker in the USAF. He reported to his first duty assignment, Whiteman AFB, MO, and began serving as an Aircraft Maintenance and Munitions Officer, working on the B-2 Stealth Bomber. While at Whiteman, Rick completed the Aircraft Maintenance and Munitions Officer Course (AMMOC – Distinguished Graduate), Nuclear Weapons Maintenance Officer Course (NMOC), and the Dynamics of International Terrorism (DIT) course. In May 99 Rick was promoted to 1st Lieutenant. Rick's assignment at Whiteman AFB came to quite a culmination as the Assistant 509th Maintenance Squadron Production Supervisor, responsible for overseeing all night shift aircraft maintenance and munitions production

in a 700+ person unit. This responsibility allowed 1Lt Noecker to play an integral part in the first ever combat employment of the B-2 stealth Bomber in March 1999 during Operation Allied Force (OAF).

Rick's next assignment was the 831st Munitions Support Squadron, Ghedi Air Base, Italy, as a Munitions Maintenance/Emergency Action Officer. Rick successfully completed United States Air Force Europe (USAFE) Command and Control training. In May 00 he was promoted to the rank of Captain. His efforts were crucial to the 831st MUNSS passing the most demanding inspection in all of USAFE; the USAFE Nuclear Surety Inspection, of which, on average, only 50% of units pass without reinspection. Rick was also the Protestant Chapel coordinator for Ghedi AB. In June 01 Rick separated from active duty to pursue his M.S. and Ph.D. in Materials Science and Engineering at Lehigh University.

During his first two years back at Lehigh Rick has received the Grand Prize (Jacquet-Lucas award) at the 2002 and 2003 International Metallographic Competition for his posters entitled "Cracking Susceptibility of AISI 1013 Steel – Cu Alloys" and "Effect of Homogenization Heat Treatment on Critical Pitting Temperature and Sigma Phase Formation in Super Duplex Stainless Steel". In January 2003, Rick passed the PhD Qualifying Exam required by the Department of Materials Science and Engineering, establishing his status as a PhD candidate at Lehigh University. In January 2003, Rick passed the PhD Qualifying Exam required by the Department of Materials Science and Engineering, establishing his status as a PhD candidate.

END OF TITLE